Symmetry of binding in doped antiferromagnets

Piotr Wróbel
Institute of Low Temperature and Structure Research, P.O. Box 937, 50-950 Wrocław 2, Poland

Robert Eder
Institut für Theoretische Physik, Universität Würzburg, Am Hubland, 97074 Würzburg, Germany

(Received 24 April 1998)

Using variational wave functions the construction of which is based on the ''string'' or ''spin bag'' picture, we calculate the energies of two-hole states classified according to the momentum and the different irreducible representations of the C_{4v} point group. We study different ratios J/t, interesting from the experimental viewpoint, and compare our results to exact diagonalization. The energetically most favorable pair symmetries are $d_{x^2-y^2}$ and p like. The mechanism of hole binding is the caterpillar-type motion of two holes connected by a string of spin defects, whereas the well-known ''broken bond'' mechanism does not produce binding for $t/J>0/4$. [S0163-1829(98)05442-3]

I. INTRODUCTION

The high-T_c cuprate materials display the basic connection between antiferromagnetism and superconductivity. This fundamental property must be explained by any convincing theory. That conviction has led to an attempt to formulate a unified theory of superconductivity and antiferromagnetism based on SO(5) symmetry.[1] Some recent numerical results[2,3] additionally support SO(5) symmetry as a concept that unifies superconductivity and antiferromagnetism. We devote ourselves to a slightly different question as to why interaction of holes with antiferromagnetic environment favors particular symmetries of bound pairs.

The simplest Hamiltonian that may be expected to contain the key features of a doped Mott-Hubbard insulator and be capable of resolving some of the numerous anomalies of cuprate superconductors is the t-J model:

$$H=-t\sum_{\langle i,j\rangle,\sigma}(\hat{c}^{\dagger}_{i,\sigma}\hat{c}_{j,\sigma}+\text{H.c.})+J\sum_{\langle i,j\rangle}\left(\mathbf{S}_i\mathbf{S}_j-\frac{n_i n_j}{4}\right). \quad (1)$$

The $\mathbf{S_i}$ are electronic spin operators, $\hat{c}^{\dagger}_{i,\sigma}=c^{\dagger}_{i,\sigma}(1-n_{i,-\sigma})$ and the sum over $\langle i,j\rangle$ stands for a summation over all pairs of nearest neighbors.

Numerical evidence suggests[4] that for hole densities $\rho_h>0.3$ the ground state of the t-J model conforms to the conventional theory of the Fermi liquid. It is not true, however, for smaller densities, $\rho_h\leqq 0.25$. In that region the density excitations resemble those of condensed bosons with characteristic energy scale t, while the spin excitations have fermionic character with the characteristic energy scale J.[5] The low doping behavior of the system may be naturally explained within the spin bag[6] or string[7–10] picture. The one-to-one mapping between the fermionic degrees of freedom in the low-energy sector of the model and a system of spin-1/2 quasiparticles may be established.[11] The effective Hamiltonian for those quasiparticles consists of a term that is related to next-nearest-neighbor hopping and terms that represent exchange and attractive nearest-neighbor density-density interactions. A similar Hamiltonian was proposed also by Dagotto, Nazarenko, and Moreo.[12] Such a Hamiltonian in a more general, however implicit form that represented many ways in which two dressed holes in an antiferromagnetic environment interact with each other,[13,14] was also discussed for the one- and two-hole problem.[15,16] The effective interaction of three holes. (three-body terms), which is relevant to the issue of phase separation was derived for the one-dimensional t-J model in a staggered magnetic field.[17]

The necessity of understanding weakly doped antiferromagnets in terms of an effective Hamiltonian follows from the failure of the Fermi-liquid-like calculations, based on the Fermi surface consistent with the local-density approximation, to describe the doping dependence of either dc resistivity or the Hall constant on the hole concentration. Experimental results for both quantities suggest that the carrier density is proportional to the hole concentration.[18] The later feature is at odds with the local-density approximation, which leads to a conclusion that transport is electronic in origin.

Many properties of the high-temperature superconductors, such as the penetration depth, the Knight shift and the nuclear relaxation rate T_1^{-1} are consistent with a $d_{x^2-y^2}$ gap. Angle-resolved photoemission spectroscopy (ARPES) measurements find evidence for a highly anisotropic gap, which can be interpreted in terms of $d_{x^2-y^2}$ symmetry. Superconducting quantum interference device (SQUID) interference experiments, corner Josephson junction studies, and flux quantization measurements in grain boundary rings are also consistent with a $d_{x^2-y^2}$ gap. Interpretation of some experiments in terms of a mixed $s+d$ state seems, however to be more appropriate. The majority of superconducting copper-oxide compounds has an orthorhombic structure. Mixing of $d_{x^2-y^2}$ with other symmetries is well understood in that case, because gap functions may not be classified according to the different irreducible representations of D_{4h}. On the other hand, the orthorhombic distortion is rather weak, and the gap function should be very reminiscent of a function that belongs to an irreducible representation of D_{4h}. Moreover, the superconducting $La_{2-x}Sr_xCuO_4$ compound is in the tetrago-

nal phase for $x>0.4$, hence one might argue that the orthorhombic distortion in not crucial to the origin of superconductivity. In these circumstances, discussion of Hamiltonians that possess the full symmetry of D_{4h}, like the t-J model, seems to be acceptable.

Our aim is to study interaction of quasiparticles in the moderately doped t-J model, that is, in the presence of antiferromagnetic correlations, and explore the structure of bound pairs by comparing the results of an exact diagonalization with an analysis in the framework of the string or spin bag approach. We concentrate on the symmetry of the wave functions of a hole pair in order to understand why antiferromagnetic correlations favor states that belong to particular representations of D_{4h}.

In the earliest version of the spin bag picture originally proposed by Schrieffer, Wen, and Zhang[6] for the Hubbard model, an added hole weakens the antiferromagnetic correlations, creating a region that can be shared by another hole. The rise in energy that is caused by a depression of the staggered magnetization surrounding the hole may be reduced in such a way. In the opposite limit $U>W$, where the Hubbard model is basically equivalent to the t-J model, a similar mechanism is operating. The binding energy of two holes with antiparallel spins in the t-J model was calculated by means of the spin bag approach and results of various extensive numerical calculations were reproduced with reasonable accuracy.[13,16] Those calculations, however, did not cover all representations of D_{4h}, because they did not take into account the full possible internal structure of spin bags. In a study of the one-dimensional t-J model in a staggered magnetic field, the variational Hilbert space included wave functions that represented all different ''orbital states'' of spin bags.[17] That extension was crucial to achievement of good agreement with the exact diagonalization. In our variational calculation we concentrate on the 4×4 cluster; however, the spin bag approach is also applicable to the infinite lattice. It would be also possible to compare results of the analytical method with simulations on slightly larger clusters but the 4×4 cluster is particularly suitable for visualization and analysis of finite-size effects.

II. SPIN BAG STATES

A pronounced separation of energy scales in the motion of doped holes is the basic assumption of our variational calculation. A mobile hole that is created at some site in a Néel-ordered spin state feels an effective potential due to formation of strings.[19,7] Coherent hole propagation becomes possible only due to the relaxation of the string of defects by means of the quantum fluctuations of the spin system. Hole motion is therefore the superposition of two very different dynamics: the rapid incoherent zigzag motion of the self-trapped hole on the energy scale t, and superimposed onto this, the coherent motion on an energy scale J that is enabled by the relaxation of the strings. This separation of energy scales manifests itself by the fact that the creation of a single hole in an antiferromagnet lowers the kinetic energy by a large and nearly **k**-independent amount amount t (which stems from the incoherent zigzag motion) whereas the dispersion of the low energy states (which stems from the coherent motion) rigorously scales with J.[20]

We start to describe the twofold dynamics of holes by constructing a family of operators, that move a hole by one lattice spacing, and by definition decrease the staggered magnetization by 1 (A denotes the $\uparrow$ sublattice and $i\in A$):

$$T_{\langle i,j\rangle}=(c^{\dagger}_{i,\downarrow}c_{j,\downarrow}+c^{\dagger}_{j,\uparrow}c_{i,\uparrow}). \tag{2}$$

We also consider m holes created at some sites $i_1,\ldots,i_m$ in the Néel state with n upturned spins at some sites $j_1,\ldots,j_n$. Acting consecutively with the operators $T_{\langle i,j\rangle}$, we obtain string states, where each hole is connected to its ''starting point'' by a trace of misaligned spins. We denote such a state as $|\{(i_k,\mathcal{P}_k)\},\{j_l\}\rangle$ where $\mathcal{P}_k$ parameterizes the geometry of the path that has taken the hole created at the site i_k. String states with the same set of ''initial sites'' $\{i_k\}$ and the same set $\{j_l\}$ of sites where spins were upturned are coupled by the hopping term; a superposition of such states therefore describes holes trapped at the sites $\{i_k\}$. As mentioned above the key assumption of our approach is the separation of energy scales between the rapid incoherent zigzag motion of the self-trapped holes and the slow coherent motion mediated by spin fluctuations. In order to describe the coherent zigzag motion we define a state with m holes trapped at the sites $i_1,\ldots,i_m$ by the ansatz

$$|\Psi_{\{i_k\},\{j_l\}}\rangle=\sum_{\{\mathcal{P}_k\}}\alpha_{\{(i_k,\mathcal{P}_k)\},\{j_l\}}|\{(i_k,\mathcal{P}_k)\},\{j_l\}\rangle. \tag{3}$$

The coefficients $\alpha_{\{(i_k,\mathcal{P}_k)\},\{j_l\}}$ are determined such that $|\Psi_{\{i_k\},\{j_l\}}\rangle$ is an eigenstate of a Hamiltonian H' that represents dynamics of the self-trapped holes:

$$H'|\Psi_{\{i_k\},\{j_l\}}\rangle=E_{\{i_k\},\{j_l\}}|\Psi_{\{i_k\},\{j_l\}}\rangle. \tag{4}$$

In H' all processes which lead to relaxation of strings have been neglected. We also assume at this stage that paths $\{\mathcal{P}_k\}$ do not cross, that is, we solve effectively the problem of a self-trapped hole on the Bethe lattice with the coordination number $z=4$. The relaxation of strings and crossing of paths give rise to effective overlap and Hamiltonian matrices which describe the coherent motion of holes. The problem defined by Eqs. (3) and (4) has its ''internal'' symmetry determined by the configuration of the sites $\{i_k\}$ and $\{j_l\}$. In the case of a single hole created at a site i and no upturned spins that symmetry contains all permutations of paths that begin at i. We shall use states which belong to some irreducible representations corresponding to those internal symmetries in order to construct irreducible representations of the small group for values of the total momentum allowed by the shape of the cluster.

Since each hole is trapped within a typical length λ [which scales as $(t/J)^{1/3}$] around its starting point i_k, the holes will feel the presence of other holes or upturned spins only if the distance of their starting points is smaller than λ or if there are some upturned spins within that range. If the distances between the ''starting points'' $\{i_k\}$ in Eq. (3) are pairwise larger than λ, Eq. (4) is solved to good approximation by a product *ansatz*,

$$\alpha_{\{(i_k,\mathcal{P}_k)\},\{j_l\}}=\prod_k\alpha^{\tau_k}_{(i_k,\mathcal{P}_k),\{j_{k,l}\}}, \tag{5}$$

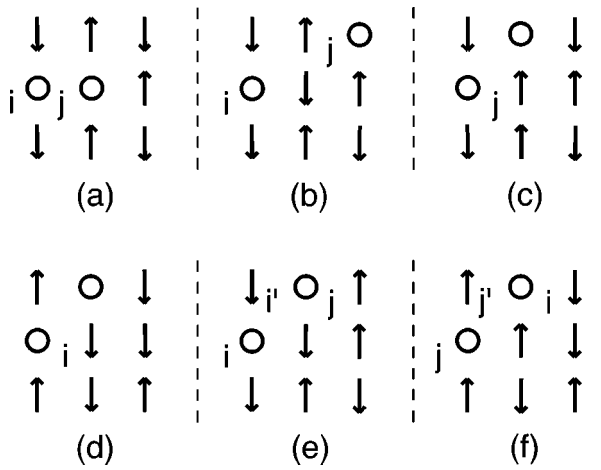

FIG. 1. Initial configurations of holes and spins related to spin polaron states: (a) $-|\Phi^{s}_{i,\hat{\mathbf{x}}}\rangle$, (b) $-|\Phi^{s}_{i,2\hat{\mathbf{x}}+\hat{\mathbf{y}}}\rangle$, (c) $-|\Phi^{(1)}_{j;\hat{\mathbf{x}},\hat{\mathbf{y}}}\rangle$, (d) $-|\Phi^{(1)}_{i;\hat{\mathbf{x}},\hat{\mathbf{y}}}\rangle$, (e) $-|\Phi^{(2)}_{i;\hat{\mathbf{x}}+\hat{\mathbf{y}},2\hat{\mathbf{x}}+\hat{\mathbf{y}}}\rangle$, (f) $-|\Phi^{(1)}_{j;\hat{\mathbf{x}}+\hat{\mathbf{y}},2\hat{\mathbf{x}}+\hat{\mathbf{y}}}\rangle$, where i and j belong, respectively, to the even and odd sublattices.

$$E_{\{i_k\},\{j_l\}}=E^{(0)}_{\{j_{0,l}\}}+\sum_{k'} E^{\tau'_k}_{i'_k,\{j_{k',l}\}}, \tag{6}$$

where $\alpha^{\tau}_{(i_k,\mathcal{P}_k),\{j_{k,l}\}}$ ($E^{\tau}_{i_k,\{j_{k,l}\}}$) are the expansion coefficients (eigenenergies) for the τth eigenstate of a single-hole self-trapped in an antiferromagnet with spins upturned at the sites $j_{k,1},j_{k,2},\ldots$. They can be computed from a Schrödinger equation that is discussed in the Appendix A. $E^{(0)}_{\{j_{0,l}\}}$ denotes the contribution to the energy from upturned spins at the sites $j_{0,1},j_{0,2},\ldots$ outside the range of motion of all holes.

If one pair of sites i,j is close to each other, but still far from the other ones, the two holes will only feel the presence of each other. In this case a Schrödinger equation for two holes has to be solved (see the Appendix A). Then the two-particle state and the eigenvalue of the two-particle Schrödinger equation have to replace the respective quantities in Eq. (6). This procedure is readily generalized to the case of an arbitrary number of groups of several holes that are clustering together.

The solution of Eq. (4) with a lowest energy $E_{\{i_k\},\{j_l\}}$ is evidently given by the totally symmetric state (3), which is invariant under all group operations related to the internal symmetry. In that case the coefficients $\alpha_{\{(i_k,\mathcal{P}_k\},\{j_l\}}$ depend only on the lengths $l(\mathcal{P}_k)$ of paths $\mathcal{P}_k$:

$$\alpha_{\{(i_k,\mathcal{P}_k)\},\{j_l\}}=\alpha_{\{(i_k,l(\mathcal{P}_k))\},\{j_l\}}. \tag{7}$$

In order to apply this construction to the problem of two holes with antiparallel spins on the 4×4 cluster we notice that there are only two different nonequivalent configurations of starting points if we require that the holes should be originally created at sites that belong to different sublattices. One category of starting points is composed of all nearest-neighbor pairs. $|\Phi^{s}_{i,\pm\hat{\mathbf{x}}(\pm\hat{\mathbf{y}})}\rangle$ denotes the most symmetric state (3) which represents two holes initially created at such a pair of sites i,j in the Néel state with no upturned spins: $\mathbf{R}_j-\mathbf{R}_i=\pm\hat{\mathbf{x}}(\pm\hat{\mathbf{y}})$ and i belongs to the spin-up sublattice. Figure 1(a) depicts the initial configuration of holes and spins related to the state $|\Phi^{s}_{i,\hat{\mathbf{x}}}\rangle$. The coefficients $\alpha_{\{(i,\mathcal{P}_i),(j,\mathcal{P}_j)\},\{\varnothing\}}$ in the expansion (3) for that state depend only on length of paths $\alpha_{\{(i,\mathcal{P}_i),(j,\mathcal{P}_j)\},\{\varnothing\}}=\tilde{\alpha}_{l(\mathcal{P}_i),l(\mathcal{P}_j)}$. The second class of starting points contains sites i, j such that $\mathbf{R}_j-\mathbf{R_i}=2\hat{x}+\hat{y}$, together with all analogous pairs which may be obtained by acting with symmetry transformations of the 4×4 cluster. Fig. 1(b) depicts the initial configuration of holes and spins related to the state $|\Phi^{s}_{i,2\hat{\mathbf{x}}+\hat{\mathbf{y}}}\rangle$. The coefficients $\alpha_{\{(i,\mathcal{P}_i),(j,\mathcal{P}_j)\},\{\varnothing\}}$ in the definition (3) of a state with the lowest energy are given to good approximation by the product $\tilde{\alpha}_{l(\mathcal{P}_i)}\tilde{\alpha}_{l(\mathcal{P}_j)}$, where $\tilde{\alpha}_{l(\mathcal{P})}$ is the totally symmetric solution for Eq. (4) in the case of a single hole. $|\Phi^{s}_{i,2\hat{\mathbf{x}}\pm\hat{\mathbf{y}}(2\hat{\mathbf{y}}\pm\hat{\mathbf{x}})}\rangle$ denotes the corresponding state. The second argument in the subscript is equal to the difference: $\mathbf{R}_j-\mathbf{R}_i$. We do not take into account states $|\Phi^{s}_{i,-2\hat{\mathbf{x}}\pm\hat{\mathbf{y}}(-2\hat{\mathbf{y}}\pm\hat{\mathbf{x}})}\rangle$ because the vector $-2\hat{\mathbf{x}}\pm\hat{\mathbf{y}}(-2\hat{\mathbf{y}}\pm\hat{\mathbf{x}})$ is an equivalent of the vector $2\hat{\mathbf{x}}\pm\hat{\mathbf{y}}(2\hat{\mathbf{y}}\pm\hat{\mathbf{x}})$ in the 4×4 cluster with periodic boundary conditions.

Due to the high symmetry of $|\Phi^{s}_{i,\pm\hat{\mathbf{x}}(\pm\hat{\mathbf{y}})}\rangle$ and $|\Phi^{s}_{i,2\hat{\mathbf{x}}\pm\hat{\mathbf{y}}(2\hat{\mathbf{y}}\pm\hat{\mathbf{x}})}\rangle$ it is impossible to construct all irreducible representations of small groups of the wave vector $\mathbf{k}$ by using just these functions. To obtain less symmetric counterparts of $|\Phi^{s}_{i,\pm\hat{\mathbf{x}}(\pm\hat{\mathbf{y}})}\rangle$ we consider as a first (initial) state in the sum (3), the Néel state with a spin upturned at a site j and two holes created at two nearest neighbors i_1 and i_2. The links between the sites i_1-j and i_2-j form a right angle, that is, $\mathbf{R}_{i_1}-\mathbf{R}_j=\pm\hat{\mathbf{x}}$, $\mathbf{R}_{i_2}-\mathbf{R}_j=\pm\hat{\mathbf{y}}$. $|\Phi^{(1)}_{j;\pm\hat{\mathbf{x}},\pm\hat{\mathbf{y}}}\rangle$ denotes a state with coefficients $\alpha_{\{(i_1,\mathcal{P}_1),(i_2,\mathcal{P}_2)\},\{j\}}=\hat{\alpha}_{l(\mathcal{P}_1),l(\mathcal{P}_2)}$ that depend only on length of paths $l(\mathcal{P}_1)$, $l(\mathcal{P}_2)$. Figures 1(c) and 1(d) depict the initial configurations of holes and spins related to the states $|\Phi^{(1)}_{j;-\hat{\mathbf{x}},\hat{\mathbf{y}}}\rangle$ and $|\Phi^{(1)}_{i;-\hat{\mathbf{x}},\hat{\mathbf{y}}}\rangle$, where i and j belong, respectively, to the even and odd sublattices. By choosing the antiferromagnetic state with two holes created at sites i, i' and a spin upturned at a site j, where $\mathbf{R}_{i'}-\mathbf{R}_i=\pm\hat{\mathbf{x}}\pm\hat{\mathbf{y}}$ and $\mathbf{R}_j-\mathbf{R}_i=\mathbf{R}_{i'}-\mathbf{R}_i+[(\mathbf{R}_{i'}-\mathbf{R}_i)\hat{\mathbf{x}}]\hat{\mathbf{x}}$ or $\mathbf{R}_j-\mathbf{R}_i=\mathbf{R}_{i'}-\mathbf{R}_i+[(\mathbf{R}_{i'}-\mathbf{R}_i)\hat{\mathbf{y}}]\hat{\mathbf{y}}$, as a first state in the sum (3), we construct a less symmetric counterpart of $|\Phi^{s}_{i,2\hat{\mathbf{x}}\pm\hat{\mathbf{y}}(2\hat{\mathbf{y}}\pm\hat{\mathbf{x}})}\rangle$. We shall use the notation $|\Phi^{(2)}_{i;\mathbf{R}_{i_{i'}}-\mathbf{R}_i,\mathbf{R}_j-\mathbf{R}_i}\rangle$ for such states. Figures 1(e) and 1(f) depict the initial configurations of holes and spins related to the states $|\Phi^{(2)}_{i;\hat{\mathbf{x}}+\hat{\mathbf{y}},2\hat{\mathbf{x}}+\hat{\mathbf{y}}}\rangle$ and $|\Phi^{(2)}_{j;\hat{\mathbf{x}}+\hat{\mathbf{y}},2\hat{\mathbf{x}}+\hat{\mathbf{y}}}\rangle$, where i and j belong, respectively, to the even and odd sublattices. Our assumption, by analogy with $|\Phi^{s}_{i,2\hat{\mathbf{x}}\pm\hat{\mathbf{y}}(2\hat{\mathbf{y}}\pm\hat{\mathbf{x}})}\rangle$, is that coefficients $\alpha_{\{(i,\mathcal{P}),(i',\mathcal{P}')\},\{j\}}$ in the expansion (3) may be factorized:

$$\alpha_{\{(i,\mathcal{P}),(i',\mathcal{P}')\},\{j\}}=\alpha_{\{(i,\mathcal{P}),\},\{\varnothing\}}\alpha_{\{(i',\mathcal{P}')\},\{j\}}, \tag{8}$$

where $\alpha_{\{(i,\mathcal{P}),\},\{\varnothing\}}$ and $\alpha_{\{(i',\mathcal{P}')\},\{j\}}$ are, respectively, a solution of the Schrödinger equation (4) in the case of a single hole, no upturned spins and a solution for a single hole initially created at a nearest neighbor of a site with an upturned spin. In both cases the ground state possess the highest possible symmetry, so that the coefficients $\alpha_{\{(i,\mathcal{P}),\},\{\varnothing\}}$ and $\alpha_{\{(i',\mathcal{P}')\},\{j\}}$ depend only on length of paths $\mathcal{P}$ and $\mathcal{P}'$:

$$\alpha_{\{(i,\mathcal{P}),\},\{\varnothing\}}=\tilde{\alpha}_{l(\mathcal{P})}, \tag{9}$$

$$\alpha_{\{(i',\mathcal{P}')\},\{j\}}=\hat{\alpha}_{l(\mathcal{P}')}. \tag{10}$$

TABLE I. Variational wave functions that realize irreducible representations of small groups of $\mathbf{k}$ in terms of functions $|\Phi^s_{i,\pm\hat{\mathbf{x}}(\pm\hat{\mathbf{y}})}\rangle$ and $|\Phi^s_{i,2\hat{\mathbf{x}}\pm\hat{\mathbf{y}}(2\hat{\mathbf{y}}\pm\hat{\mathbf{x}})}\rangle$.

$\mathbf{k}$	Representation (group)	Wave function
0	$A_1(C_{4v})$	$\frac{1}{\sqrt{N/2}}\Sigma_{i\in A}[a(\lvert\Phi^s_{i,\hat{\mathbf{x}}}\rangle+\lvert\Phi^s_{i,-\hat{\mathbf{x}}}\rangle+\lvert\Phi^s_{i,\hat{\mathbf{y}}}\rangle+\lvert\Phi^s_{i,-\hat{\mathbf{y}}}\rangle)+b(\lvert\Phi^s_{i,2\hat{\mathbf{x}}+\hat{\mathbf{y}}}\rangle+\lvert\Phi^s_{i,2\hat{\mathbf{x}}-\hat{\mathbf{y}}}\rangle+\lvert\Phi^s_{i,2\hat{\mathbf{y}}+\hat{\mathbf{x}}}\rangle+\lvert\Phi^s_{i,2\hat{\mathbf{y}}-\hat{\mathbf{x}}}\rangle)]$
0	$B_1(C_{4v})$	$\frac{1}{\sqrt{N/2}}\Sigma_{i\in A}[a(\lvert\Phi^s_{i,\hat{\mathbf{x}}}\rangle+\lvert\Phi^s_{i,-\hat{\mathbf{x}}}\rangle-\lvert\Phi^s_{i,\hat{\mathbf{y}}}\rangle-\lvert\Phi^s_{i,-\hat{\mathbf{y}}}\rangle)+b(\lvert\Phi^s_{i,2\hat{\mathbf{x}}+\hat{\mathbf{y}}}\rangle+\lvert\Phi^s_{i,2\hat{\mathbf{x}}-\hat{\mathbf{y}}}\rangle-\lvert\Phi^s_{i,2\hat{\mathbf{y}}+\hat{\mathbf{x}}}\rangle-\lvert\Phi^s_{i,2\hat{\mathbf{y}}-\hat{\mathbf{x}}}\rangle)]$
0	$E(C_{4v})$	$\frac{1}{\sqrt{N/2}}\Sigma_{i\in A}[a(\lvert\Phi^s_{i,\hat{\mathbf{x}}}\rangle-\lvert\Phi^s_{i,-\hat{\mathbf{x}}}\rangle)+b(\lvert\Phi^s_{i,2\hat{\mathbf{y}}+\hat{\mathbf{x}}}\rangle-\lvert\Phi^s_{i,2\hat{\mathbf{y}}+\hat{\mathbf{x}}}\rangle)]$
$(\pi,0)$	$A_1(C_{2v})$	$\frac{1}{\sqrt{N/2}}\Sigma_{i\in A}e^{i\mathbf{k}\mathbf{R}_i}[a_1(\lvert\Phi^s_{i,\hat{\mathbf{x}}}\rangle+\lvert\Phi^s_{i,-\hat{\mathbf{x}}}\rangle)+a_2(\lvert\Phi^s_{i,\hat{\mathbf{y}}}\rangle+\lvert\Phi^s_{i,-\hat{\mathbf{y}}}\rangle)+b_1(\lvert\Phi^s_{i,2\hat{\mathbf{x}}+\hat{\mathbf{y}}}\rangle+\lvert\Phi^s_{i,2\hat{\mathbf{x}}-\hat{\mathbf{y}}}\rangle)+b_2(\lvert\Phi^s_{i,2\hat{\mathbf{y}}+\hat{\mathbf{x}}}\rangle+\lvert\Phi^s_{i,2\hat{\mathbf{y}}-\hat{\mathbf{x}}}\rangle)]$
$(\pi,0)$	$B_1(C_{2v})$	$\frac{1}{\sqrt{N/2}}\Sigma_{i\in A}e^{i\mathbf{k}\mathbf{R}_i}[a(\lvert\Phi^s_{i,\hat{\mathbf{y}}}\rangle-\lvert\Phi^s_{i,-\hat{\mathbf{y}}}\rangle)+b(\lvert\Phi^s_{i,2\hat{\mathbf{x}}+\hat{\mathbf{y}}}\rangle-\lvert\Phi^s_{i,2\hat{\mathbf{x}}-\hat{\mathbf{y}}}\rangle)]$
$(\pi,0)$	$B_2(C_{2v})$	$\frac{1}{\sqrt{N/2}}\Sigma_{i\in A}e^{i\mathbf{k}\mathbf{R}_i}[a(\lvert\Phi^s_{i,\hat{\mathbf{x}}}\rangle-\lvert\Phi^s_{i,-\hat{\mathbf{x}}}\rangle)+b(\lvert\Phi^s_{i,2\hat{\mathbf{y}}+\hat{\mathbf{x}}}\rangle-\lvert\Phi^s_{i,2\hat{\mathbf{y}}-\hat{\mathbf{x}}}\rangle)]$
$(\pi/2,\pi/2)$	$A_1(C_s)$	$\frac{1}{\sqrt{N/2}}\Sigma_{i\in A}e^{i\mathbf{k}\mathbf{R}_i}[a_1(\lvert\Phi^s_{i,\hat{\mathbf{x}}}\rangle+\lvert\Phi^s_{i,\hat{\mathbf{y}}}\rangle)+a_2(\lvert\Phi^s_{i,-\hat{\mathbf{x}}}\rangle+\lvert\Phi^s_{i,-\hat{\mathbf{y}}}\rangle)+b_1(\lvert\Phi^s_{i,2\hat{\mathbf{x}}+\hat{\mathbf{y}}}\rangle+\lvert\Phi^s_{i,2\hat{\mathbf{y}}+\hat{\mathbf{x}}}\rangle)+b_2(\Phi^s_{i,2\hat{\mathbf{x}}-\hat{\mathbf{y}}}\rangle+\lvert\Phi^s_{i,2\hat{\mathbf{y}}-\hat{\mathbf{x}}}\rangle)]$
$(\pi/2,\pi/2)$	$A_2(C_s)$	$\frac{1}{\sqrt{N/2}}\Sigma_{i\in A}e^{i\mathbf{k}\mathbf{R}_i}[a_1(\lvert\Phi^s_{i,\hat{\mathbf{x}}}\rangle-\lvert\Phi^s_{i,\hat{\mathbf{y}}}\rangle)+a_2(\lvert\Phi^s_{i,-\hat{\mathbf{x}}}\rangle-\lvert\Phi^s_{i,-\hat{\mathbf{y}}}\rangle)+b_1(\lvert\Phi^s_{i,2\hat{\mathbf{x}}+\hat{\mathbf{y}}}\rangle-\lvert\Phi^s_{i,2\hat{\mathbf{y}}+\hat{\mathbf{x}}}\rangle)+b_2(\lvert\Phi^s_{i,2\hat{\mathbf{x}}-\hat{\mathbf{y}}}\rangle-\lvert\Phi^s_{i,2\hat{\mathbf{y}}-\hat{\mathbf{x}}}\rangle)]$
$(\pi/2,0)$	$A_1(C_s)$	$\frac{1}{\sqrt{N/2}}\Sigma_{i\in A}e^{i\mathbf{k}\mathbf{R}_i}[a_1\lvert\Phi^s_{i,\hat{\mathbf{x}}}\rangle+a_2\lvert\Phi^s_{i,-\hat{\mathbf{x}}}\rangle+a_3(\lvert\Phi^s_{i,\hat{\mathbf{y}}}\rangle+\lvert\Phi^s_{i,-\hat{\mathbf{y}}}\rangle)+b_1(\lvert\Phi^s_{i,2\hat{\mathbf{x}}+\hat{\mathbf{y}}}\rangle+\lvert\Phi^s_{i,2\hat{\mathbf{x}}-\hat{\mathbf{y}}}\rangle)+b_2\lvert\Phi^s_{i,2\hat{\mathbf{y}}+\hat{\mathbf{x}}}\rangle+b_3\lvert\Phi^s_{i,2\hat{\mathbf{y}}-\hat{\mathbf{x}}}\rangle]$
$(\pi/2,0)$	$A_2(C_s)$	$\frac{1}{\sqrt{N/2}}\Sigma_{i\in A}e^{i\mathbf{k}\mathbf{R}_i}[a(\lvert\Phi^s_{i,\hat{\mathbf{y}}}\rangle-\lvert\Phi^s_{i,-\hat{\mathbf{y}}}\rangle)+b(\lvert\Phi^s_{i,2\hat{\mathbf{x}}+\hat{\mathbf{y}}}\rangle-\lvert\Phi^s_{i,2\hat{\mathbf{x}}-\hat{\mathbf{y}}}\rangle)]$

III. VARIATIONAL WAVE FUNCTIONS

We have to consider few $\mathbf{k}$ points in the Brillouin zone because many of them are either related by symmetry transformations or differ by the antiferromagnetic wave vector $\mathbf{Q}=(\pi,\pi)$. By choosing an antiferromagnet as a medium in which holes propagate and interact we have effectively reduced the size of the Brillouin zone so that the momenta $\mathbf{k}$ and $\mathbf{k}+\mathbf{Q}$ are equivalent. Table I gives the variational wave functions that realize some irreducible representations of small groups of $\mathbf{k}$ in terms of the functions $|\Phi^s_{i,\pm\hat{\mathbf{x}}(\pm\hat{\mathbf{y}})}\rangle$ and $|\Phi^s_{i,2\hat{\mathbf{x}}\pm\hat{\mathbf{y}}(2\hat{\mathbf{y}}\pm\hat{\mathbf{x}})}\rangle$.

Some representations can not be constructed using only those states, because their symmetry is too high. Quite generally, loss of symmetry brings rise in energy. The most symmetric solutions of Eq. (4) that allow us to construct the remaining representations are states $|\Phi^{(1)}_{l;\pm\hat{\mathbf{x}},\pm\hat{\mathbf{y}}}\rangle$ and $|\Phi^{(2)}_{l;\pm\hat{\mathbf{x}}\pm\hat{\mathbf{y}},\pm2\hat{\mathbf{x}}\pm\hat{\mathbf{y}}(\pm\hat{\mathbf{x}}\pm2\hat{\mathbf{y}})}\rangle$. The wave functions that realize the less symmetric representations in terms of the states $|\Phi^{(1)}_{l;\pm\hat{\mathbf{x}},\pm\hat{\mathbf{y}}}\rangle$ and $|\Phi^{(2)}_{l;\pm\hat{\mathbf{x}}\pm\hat{\mathbf{y}},\pm2\hat{\mathbf{x}}\pm\hat{\mathbf{y}}(\pm\hat{\mathbf{x}}\pm2\hat{\mathbf{y}})}\rangle$ are listed in Table II.

IV. INTERACTION OF SPIN POLARONS

The states (3) describe the trapping of holes in an antiferromagnetic medium by local deformation of the spin arrangement. The notion of a spin polaron is therefore applicable to them. In the previous section we have shown combinations of polaronic states with given momentum and symmetry. To calculate the energy we now need to know the following overlap and Hamiltonian matrix elements:

$$N_{\{i_k\},\{j_l\};\{i'_{k'}\},\{j'_{l'}\}}=\langle\Psi_{\{i_k\},\{j_l\}}|\Psi_{\{i'_{k'}\},\{j'_{l'}\}}\rangle, \tag{11}$$

TABLE II. Variational wave functions which realize irreducible representations of small groups of **k** in terms of functions $|\Phi^{(1)}_{l,\pm\hat{\mathbf{x}}(\pm\hat{\mathbf{y}})}\rangle$ and $|\Phi^{(2)}_{l;\pm\hat{\mathbf{x}}\pm\hat{\mathbf{y}},\pm 2\hat{\mathbf{x}}\pm\hat{\mathbf{y}}(\pm 2\hat{\mathbf{y}}\pm\hat{\mathbf{x}})}\rangle$.

k	Repr. (group)	Wave function
0	$A_2(C_{4v})$	$\frac{1}{\sqrt{N/2}}\{\Sigma_{i\in A}[a_1(\|\Phi^{(1)}_{i;\hat{\mathbf{x}},\mathbf{y}}\rangle+\|\Phi^{(1)}_{i;-\hat{\mathbf{x}},-\mathbf{y}}\rangle-\|\Phi^{(1)}_{i;\hat{\mathbf{x}},-\mathbf{y}}\rangle-\|\Phi^{(1)}_{i;-\hat{\mathbf{x}},\mathbf{y}}\rangle)+b_1(\|\Phi^{(2)}_{i;\hat{\mathbf{x}}+\hat{\mathbf{y}},2\hat{\mathbf{x}}+\hat{\mathbf{y}}}\rangle+\|\Phi^{(2)}_{i;-\hat{\mathbf{x}}-\hat{\mathbf{y}},-2\hat{\mathbf{x}}-\hat{\mathbf{y}}}\rangle+\|\Phi^{(2)}_{i;-\hat{\mathbf{x}}+\hat{\mathbf{y}},-\hat{\mathbf{x}}+2\hat{\mathbf{y}}}\rangle+\|\Phi^{(2)}_{i;\hat{\mathbf{x}}-\hat{\mathbf{y}},\hat{\mathbf{x}}-2\hat{\mathbf{y}}}\rangle-\|\Phi^{(2)}_{i;\hat{\mathbf{x}}-\hat{\mathbf{y}},2\hat{\mathbf{x}}-\hat{\mathbf{y}}}\rangle-\|\Phi^{(2)}_{i;-\hat{\mathbf{x}}+\hat{\mathbf{y}},-2\hat{\mathbf{x}}+\hat{\mathbf{y}}}\rangle-\|\Phi^{(2)}_{i;\hat{\mathbf{x}}+\hat{\mathbf{y}},\hat{\mathbf{x}}+2\hat{\mathbf{y}}}\rangle-\|\Phi^{(2)}_{i;-\hat{\mathbf{x}}-\hat{\mathbf{y}},-\hat{\mathbf{x}}-2\hat{\mathbf{y}}}\rangle)]+\Sigma_{j\notin A}[a_1\to a_2,b_1\to b_2,i\to j]\}$
0	$B_2(C_{4v})$	$\frac{1}{\sqrt{N/2}}[\Sigma_{i\in A}b_1(\|\Phi^{(2)}_{i;\hat{\mathbf{x}}+\hat{\mathbf{y}},2\hat{\mathbf{x}}+\mathbf{y}}\rangle+\|\Phi^{(2)}_{i;-\hat{\mathbf{x}}-\hat{\mathbf{y}},-2\hat{\mathbf{x}}-\mathbf{y}}\rangle+\|\Phi^{(2)}_{i;\hat{\mathbf{x}}+\hat{\mathbf{y}},\hat{\mathbf{x}}+2\mathbf{y}}\rangle+\|\Phi^{(2)}_{i;-\hat{\mathbf{x}}-\hat{\mathbf{y}},-\hat{\mathbf{x}}-2\mathbf{y}}\rangle-\|\Phi^{(2)}_{i;\hat{\mathbf{x}}-\hat{\mathbf{y}},2\hat{\mathbf{x}}-\hat{\mathbf{y}}}\rangle-\|\Phi^{(2)}_{i;-\hat{\mathbf{x}}+\hat{\mathbf{y}},-2\hat{\mathbf{x}}+\hat{\mathbf{y}}}\rangle-\|\Phi^{(2)}_{i;-\hat{\mathbf{x}}+\hat{\mathbf{y}},-\hat{\mathbf{x}}+2\hat{\mathbf{y}}}\rangle-\|\Phi^{(2)}_{i;\hat{\mathbf{x}}-\hat{\mathbf{y}},\hat{\mathbf{x}}-2\hat{\mathbf{y}}}\rangle)+\Sigma_{j\notin A}b_2(i\to j)$
$(\pi,0)$	$A_2(C_{2v})$	$\frac{1}{\sqrt{N/2}}\{\Sigma_{i\in A}e^{i\mathbf{k}\mathbf{R}_i}[a_1(\|\Phi^{(1)}_{i;\hat{\mathbf{x}},\mathbf{y}}\rangle+\|\Phi^{(1)}_{i;-\hat{\mathbf{x}},-\mathbf{y}}\rangle-\|\Phi^{(1)}_{i;\hat{\mathbf{x}},-\mathbf{y}}\rangle-\|\Phi^{(1)}_{i;-\hat{\mathbf{x}},\mathbf{y}}\rangle)+b_1(\|\Phi^{(2)}_{i;\mathbf{x}+\hat{\mathbf{y}},2\hat{\mathbf{x}}+\hat{\mathbf{y}}}\rangle+\|\Phi^{(2)}_{i;-\hat{\mathbf{x}}-\hat{\mathbf{y}},-2\hat{\mathbf{x}}-\hat{\mathbf{y}}}\rangle-\|\Phi^{(2)}_{i;\hat{\mathbf{x}}-\hat{\mathbf{y}},2\hat{\mathbf{x}}-\hat{\mathbf{y}}}\rangle-\|\Phi^{(2)}_{i;-\hat{\mathbf{x}}+\hat{\mathbf{y}},-2\hat{\mathbf{x}}+\hat{\mathbf{y}}}\rangle)+b_2(\|\Phi^{(2)}_{i;\hat{\mathbf{x}}+\hat{\mathbf{y}},\hat{\mathbf{x}}+2\hat{\mathbf{y}}}\rangle+\|\Phi^{(2)}_{i;-\hat{\mathbf{x}}-\hat{\mathbf{y}},-\hat{\mathbf{x}}-2\hat{\mathbf{y}}}\rangle-\|\Phi^{(2)}_{i;-\hat{\mathbf{x}}+\hat{\mathbf{y}},-\hat{\mathbf{x}}+2\hat{\mathbf{y}}}\rangle-\|\Phi^{(2)}_{i;\hat{\mathbf{x}}-\hat{\mathbf{y}},-\hat{\mathbf{x}}-2\hat{\mathbf{y}}}\rangle)]+\Sigma_{j\notin A}e^{i\mathbf{k}\mathbf{R}_j}[a_1\to a_2,b_1\to b_3,b_2\to b_4,i\to j]\}$

$$H_{\{i_k\},\{j_l\};\{i'_{k'}\},\{j'_{l'}\}}=\langle\Psi_{\{i_k\},\{j_l\}}|H|\Psi_{\{i'_{k'}\},\{j'_{l'}\}}\rangle, \qquad (12)$$

These will now be discussed one after another. The simplest terms in the diagonal elements of the overlap and Hamiltonian matrices come from self-overlap of states $|\Psi_{\{i_k\},\{j_l\}}\rangle$ and from their eigenenergies $E_{\{i_k\},\{j_l\}}$. During the process of construction of states $|\Psi_{\{i_k\},\{j_l\}}\rangle$ that are solutions of Eq. (4), we have made many simplifications. Crossing of paths and processes that lead to relaxation of strings have been neglected. They should now contribute to elements (11) and (12). All such new terms have been represented by a kind of diagrams depicted by Figs. 3–15. Figures 3–5 represent matrix elements that couple states $|\Phi^{s}_{i,\pm\hat{\mathbf{x}}(\pm\hat{\mathbf{y}})}\rangle$ and $|\Phi^{s}_{i,2\hat{\mathbf{x}}\pm\hat{\mathbf{y}}(2\hat{\mathbf{y}}\pm\hat{\mathbf{x}})}\rangle$, while Figs. 6–15 represent elements that couple states $|\Phi^{(1)}_{l;\pm\hat{\mathbf{x}},\pm\hat{\mathbf{y}}}\rangle$ and $|\Phi^{(2)}_{l;\pm\hat{\mathbf{x}}\pm\hat{\mathbf{y}},\pm 2\hat{\mathbf{x}}\pm\hat{\mathbf{y}}(\pm\hat{\mathbf{x}}\pm 2\hat{\mathbf{y}})}\rangle$. Open and solid circles in the right part of each figure represent starting sites of holes for both states that contribute to the matrix element and correspond to two sets of indices $\{i_k\}$ and $\{i'_{k'}\}$. Open and solid diamonds also represent two sets of sites, namely, $\{j_l\}$ and $\{j'_{l'}\}$ where spins have been upturned. Left and central parts of diagrams demonstrate how identical states can be generated from different original configurations of holes. They depict two string states $\langle\{(i_k,\mathcal{P}_k)\},\{j_l\}|$ and $|\{(i'_{k'},\mathcal{P}_{k'})\},\{j'_{l'}\}\rangle$. An arrow represents a path that a hole has followed. A curved arrow depicts action of the hopping part of the Hamiltonian on a string state. The action of the exchange part of the Hamiltonian is represented by two slanted crosses. The Appendix B explains rules for obtaining elements of the overlap and Hamiltonian matrices from diagrams presented in Figs. 3–15. Figure 2 shows, for illustration, the spin configurations related to some diagrams. We have assumed that the site in the lower left corner of each diagram belongs to the spin-up sublattice. Figure 3(a) represents overlap between two string states, which gives rise to a term in a matrix element $N_{\{i_k\},\{j_l\};\{i'_{k'}\},\{j'_{l'}\}}$ for $\{i_k\}=\{i_1,i_2\}$, $\{j_l\}=\{\varnothing\}$, $\{i'_{k'}\}=\{i_3,i_2\}$ and $\{j'_{l'}\}=\{\varnothing\}$; where $\mathbf{R}_{i_2}-\mathbf{R}_{i_1}=\pm\hat{\mathbf{x}}(\pm\hat{\mathbf{y}})$ and $\mathbf{R}_{i_3}-\mathbf{R}_{i_1}=\pm 2\hat{\mathbf{x}}(\pm 2\hat{\mathbf{y}})$. The states coupled by that element are ground states of Eq. (4) that represent holes oscillating in the vicinity of a pair of nearest-neighbor sites. They possess the highest possible symmetry: $|\{i_1,i_2\},\{\varnothing\}\rangle=|\Phi^{s}_{i_1,\pm\hat{\mathbf{x}}(\pm\hat{\mathbf{y}})}\rangle$, $|\{i_3,i_2\},\{\varnothing\}\rangle=|\Phi^{s}_{i_3,\mp\hat{\mathbf{x}}(\mp\hat{\mathbf{y}})}\rangle$. Figures 2(a) and 2(b) depict original configurations which correspond to the left and central parts of Fig. 3(a). Figure 2(c) represents the final common spin configuration that was formed after the right hole in Fig. 2(a) and the left hole in Fig. 2(b) had moved by one lattice spacing in the horizontal direction. The corresponding term in

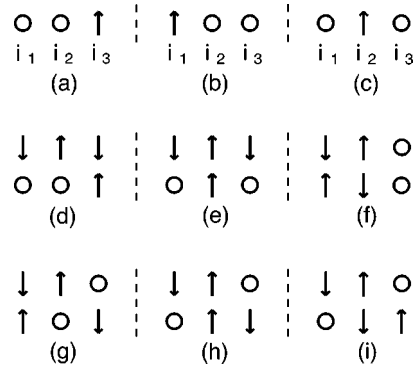

FIG. 2. Spin configurations related to some contributions to overlap and Hamiltonian matrices.

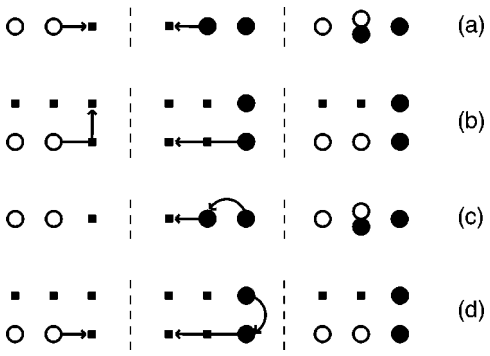

FIG. 3. Some diagrams that represent processes contributing to the overlap and Hamiltonian matrices. Matrix elements couple states $|\Phi^s_{i,\pm\hat{\mathbf{x}}(\pm\hat{\mathbf{y}})}\rangle$ and $|\Phi^s_{i,\pm 2\hat{\mathbf{x}}\pm\hat{\mathbf{y}}(\pm 2\hat{\mathbf{y}}\pm\hat{\mathbf{x}})}\rangle$.

$N_{\{i_1,i_2\},\{\emptyset\};\{i_3,i_2\},\{\emptyset\}}$ is given by $-(\tilde{\alpha}_{0,1})^2$. The minus sign originates from the order in which the holes were created in the two states represented by Figs. 2(a) and 2(b), and from correspondence between holes in the original states and the final state depicted by Fig. 2(c). Another process, shown in Fig. 3(b), contributes to the overlap matrix. Figures 2(d) and 2(f) depict the starting configurations for the states represented by the left and central parts of Fig. 3(b). The final configuration, which is common to both states, is shown in Fig. 2(h). The intermediate states are represented by Figs. 2(e) and 2(g). The central part of Fig. 3(c) depicts a hopping process that has been excluded from the Hamiltonian H' by the definition of spin polarons (3). It gives rise to a term $t\tilde{\alpha}_{0,0}\tilde{\alpha}_{0,1}$ in the element $H_{\{i_1,i_2\},\{\emptyset\};\{i_3,i_2\},\{\emptyset\}}$. The action of the kinetic part of the Hamiltonian on the state depicted in the central part of Fig. 3(a), with the coefficient $\tilde{\alpha}_{0,1}$ in the expansion (3) gives rise to the state shown in the left part of Fig. 3(c) with the coefficient $\tilde{\alpha}_{0,0}$ and a configuration of holes and spins shown in Fig. 2(a). Figure 3(d) depicts a hopping process related to the overlap of states represented by Fig. 3(b). Figure 2(e) depicts a final configuration common to states shown in the left and central parts of Fig. 3(d). There exists another new term in elements of the overlap matrix N analogous to the term represented by Fig. 3(a). That term is represented by a diagram of different shape and couples states $|\Phi^s_{i_1,\hat{\mathbf{x}}}\rangle$ and $|\Phi^s_{i_3,-\hat{\mathbf{y}}}\rangle$, where $\mathbf{R}_{i_3}-\mathbf{R}_{i_1}=\hat{\mathbf{x}}+\hat{\mathbf{y}}$; and all analogous pairs of states that may be obtained by action of symmetry transformations of the 4×4 cluster. There exist three additional new terms in elements of the overlap matrix that are represented by diagrams equivalent to Fig. 3(b) but of different shape. The diagram in Fig. 3(c) has also an equivalent and the diagram in Fig. 3(d) has four.

We proceed now to discuss processes related to the *transverse* part of the Heisenberg Hamiltonian that couple states $|\Phi^s_{i,\pm\hat{\mathbf{x}}(\pm\hat{\mathbf{y}})}\rangle$ and $|\Phi^s_{i,2\hat{\mathbf{x}}\pm\hat{\mathbf{y}}(2\hat{\mathbf{y}}\pm\hat{\mathbf{x}})}\rangle$. Diagrams which represent different categories of these are shown in Fig. 4. As an example we discuss in detail Fig. 4(c), which depicts a process coupling states $|\Phi^s_{i,\hat{\mathbf{x}}}\rangle$ and $|\Phi^s_{i,2\hat{\mathbf{x}}+\hat{\mathbf{y}}}\rangle$. The initial configurations of holes and spins for the left and central part of Fig. 4(c) are shown in Fig. 2(d) and Fig. 2(i), respectively. Figure 2(h) depicts a state created by two jumps of the right hole in the left part of Fig. 4(c). Action of the exchange part of the Heisenberg Hamiltonian [represented by the central part of

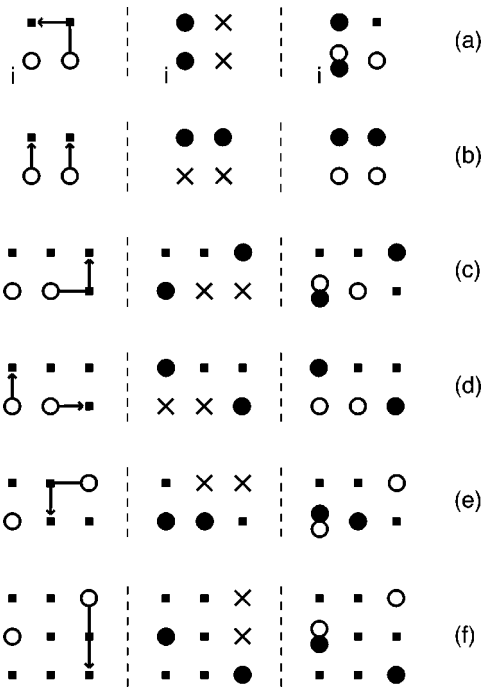

FIG. 4. Processes related to the exchange part of the Hamiltonian. Matrix elements couple states $|\Phi^s_{i,\pm\hat{\mathbf{x}}(\pm\hat{\mathbf{y}})}\rangle$ and $|\Phi^s_{i,\pm 2\hat{\mathbf{x}}\pm\hat{\mathbf{y}}(\pm 2\hat{\mathbf{y}}\pm\hat{\mathbf{x}})}\rangle$.

Fig. 4(c)], which upturns two antiparallel spins on a pair of nearest-neighbor sites, on the state depicted by Fig. 2(i) also gives rise to a state shown in Fig. 2(h). The corresponding contribution to the matrix element is given by $J/2\tilde{\alpha}_{0,2}\tilde{\alpha}_0^2$.

The periodic boundary conditions allow for some processes that are specific to the 4×4 cluster. Figure 5 contains diagrams that depict such processes. Figure 5(a), for example, represents a contribution $J/2[\tilde{\alpha}_{0,2}\tilde{\alpha}_{0,0}/(z-1)+(z-2)\Sigma_{\mu=0,\nu=2}(z-1)^{\mu+\nu-3}\tilde{\alpha}_{\mu,\nu}\tilde{\alpha}_{\mu,\nu-2}]$ to the matrix element that couples states $|\Phi^s_{i,\hat{\mathbf{x}}}\rangle$ and $|\Phi^s_{i,-\hat{\mathbf{x}}}\rangle$. Due to the periodic boundary conditions the horizontal motion of a hole in the left part of Fig. 5(a) brings that hole eventually to the other side of its neighbor. Figures 3, 4, and 5 contain examples of all possible types of processes that involve paths of total length not exceeding two lattice spacings. Many processes that have not been shown explicitly in those figures are represented by diagrams of different geometry. Nevertheless, they are ruled by the same mechanisms.

Diagrams for processes which contribute to elements of N coupling states $|\Phi^{(1)}_{l;\pm\hat{\mathbf{x}},\pm\hat{\mathbf{y}}}\rangle$ and $|\Phi^{(2)}_{l;\pm\hat{\mathbf{x}}\pm\hat{\mathbf{y}},\pm 2\hat{\mathbf{x}}\pm\hat{\mathbf{y}}(\pm\hat{\mathbf{x}}\pm 2\hat{\mathbf{y}})}\rangle$ have

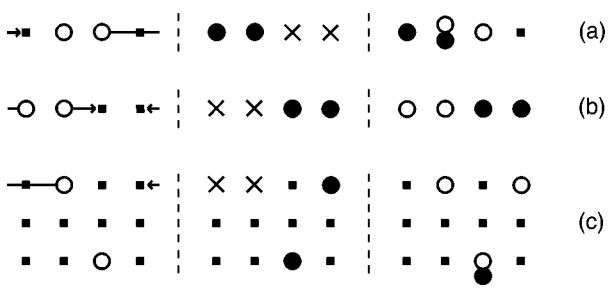

FIG. 5. Processes that couple states $|\Phi^s_{\cdot,\cdot}\rangle$ and involve effects related to periodic boundary conditions of the 4×4 cluster.

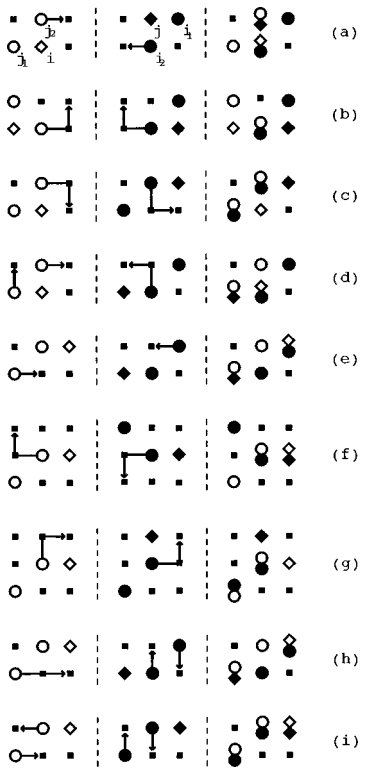

FIG. 6. Processes that give rise to contributions to matrix elements of the overlap matrix N and couple states $|\Phi^s_{i,\pm\hat{\mathbf{x}}(\pm\hat{\mathbf{y}})}\rangle$ and $|\Phi^s_{i,\pm 2\hat{\mathbf{x}}\pm\hat{\mathbf{y}}(\pm 2\hat{\mathbf{y}}\pm\hat{\mathbf{x}})}\rangle$.

been presented in Figs. 6, 7, and 8. Figure 6 depicts standard processes which give rise to contributions to the overlap matrix. The process depicted in Fig. 6(a) gives rise to a term $-\Sigma_{\mu=0,\nu=1}(z-1)^{\mu+\nu-1}\hat{\alpha}_{\mu,\nu}\hat{\alpha}_{\nu-1,\mu+1}$ in an element that couples states $|\Phi^{(1)}_{i;-\hat{\mathbf{x}},\hat{\mathbf{y}}}\rangle$ and $|\Phi^{(1)}_{j;\hat{\mathbf{x}},-\hat{\mathbf{y}}}\rangle$, where $\mathbf{R}_j-\mathbf{R}_i=\hat{\mathbf{y}}$. The minus sign is related to the fermionic character of the hole and a convention according to which holes at the sites j_1,j_2 have been created in the same order as holes at the sites i_1,i_2. Processes shown in Fig. 7 involve boundary effects. A diagram in Fig. 7(a) gives rise to a contribution $-[\tilde{\alpha}^2_2\hat{\alpha}^2_0(z-1)^{-1}+(z-2)\Sigma_{\mu=2,\nu=0}(z-1)^{\mu+\nu-3}\tilde{\alpha}_\mu\hat{\alpha}_\nu\tilde{\alpha}_{\nu+2}\hat{\alpha}_{\mu-2}]$ to an element that couples states $|\Phi^{(2)}_{l;\hat{\mathbf{x}}+\hat{\mathbf{y}},2\hat{\mathbf{x}}+\hat{\mathbf{y}}}\rangle$ and $|\Phi^{(2)}_{l;-\hat{\mathbf{x}}+\hat{\mathbf{y}},-2\hat{\mathbf{x}}+\hat{\mathbf{y}}}\rangle$. Figure 8 depicts some fictitious states which by definition contribute to states $|\Phi^{(1)}_{l;\pm\hat{\mathbf{x}},\pm\hat{\mathbf{y}}}\rangle$ and $|\Phi^{(2)}_{l;\pm\hat{\mathbf{x}}\pm\hat{\mathbf{y}},\pm 2\hat{\mathbf{x}}\pm\hat{\mathbf{y}}(\pm\hat{\mathbf{x}}\pm 2\hat{\mathbf{y}})}\rangle$, because during the process of construction of ''spin bag'' states we have neglected the possibility that paths may cross. Therefore some states that contribute to $|\Psi_{\{i_k\},\{j_l\}}\rangle$ in Eq. (3) correspond to forbidden configurations representing two holes that occupy the same

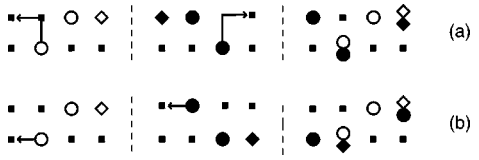

FIG. 7. Diagrammatic representation of overlap between different spin bag states. Due to periodic boundary conditions string states in the left and central parts of each diagram are equal.

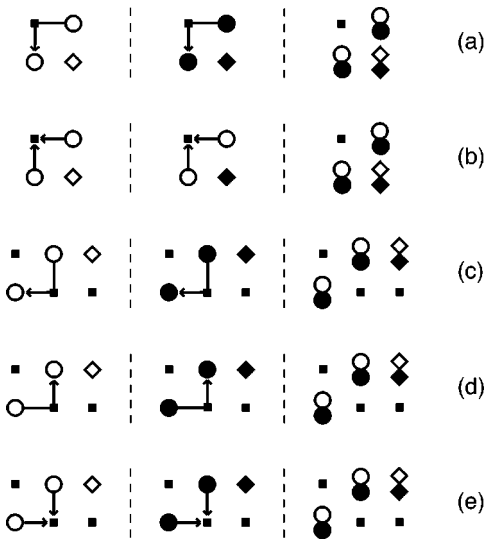

FIG. 8. Diagrams that depict some fictitious states that contribute to self-overlap of states $|\Phi^{(1)}_{l;\pm\hat{\mathbf{x}},\pm\hat{\mathbf{y}}}\rangle$ and $|\Phi^{(2)}_{l;\pm\hat{\mathbf{x}}\pm\hat{\mathbf{y}},\pm 2\hat{\mathbf{x}}\pm\hat{\mathbf{y}}(\pm\hat{\mathbf{x}}\pm 2\hat{\mathbf{y}})}\rangle$ and sums in normalization conditions (A6), (A7), and (A8).

site. Fictitious states make contributions to diagonal elements that are related to self-overlap of states $|\Psi_{\{i_k\},\{j_l\}}\rangle$ and their eigenenergies $E_{\{i_k\},\{j_l\}}$. Those contributions should therefore be subtracted at a later stage of calculations. Figure 8(a), for example, represents a subtraction $-\Sigma_{\mu=2}(z-1)^{\mu-2}\hat{\alpha}^2_{0,\mu}$ from the diagonal element for a state $|\Phi^{(1)}_{l,-\hat{\mathbf{x}},\hat{\mathbf{y}}}\rangle$.

Some contributions to the Hamiltonian matrix H originate in an obvious way from the overlap matrix N and eigenenergies $E_{\{i_k\},\{j_k\}}$ of states coupled by elements of N. The diagram in Fig. 3(a), for example, gives rise to a term $-\tilde{E}_2\Sigma_{\mu=0,\nu=1}(z-1)^{\mu+\nu-1}\tilde{\alpha}^2_{\mu,\nu}$ in a matrix element that couples states $|\Phi^s_{i,-\hat{\mathbf{x}}}\rangle$ and $|\Phi^s_{i,\hat{\mathbf{x}}}\rangle$.

The possibility that a hole that has left the initial site may occupy a site that is a nearest neighbor of another hole has not been taken into account in the Schrödinger equations for $\tilde{E}_1$, $\tilde{E}_2$, $\hat{E}_1$, and $\hat{E}_2$. On the other hand, such configurations give rise to nonstandard contributions from the diagonal term $J\Sigma_{\langle i,j\rangle}(S^z_iS^z_j-n_in_j/4)$, which are lowered by $J/2$ as compared to the case when the paths of two holes do not

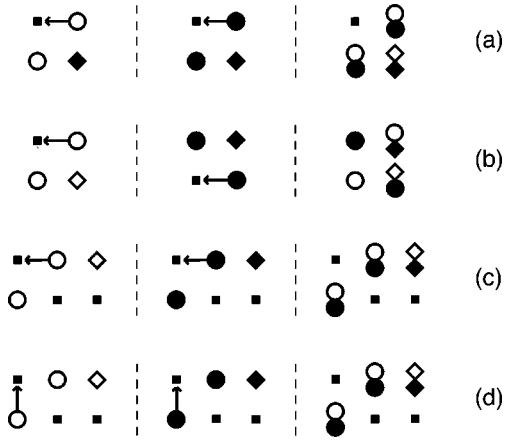

FIG. 9. Overlapping string states with reduced diagonal contribution to energy.

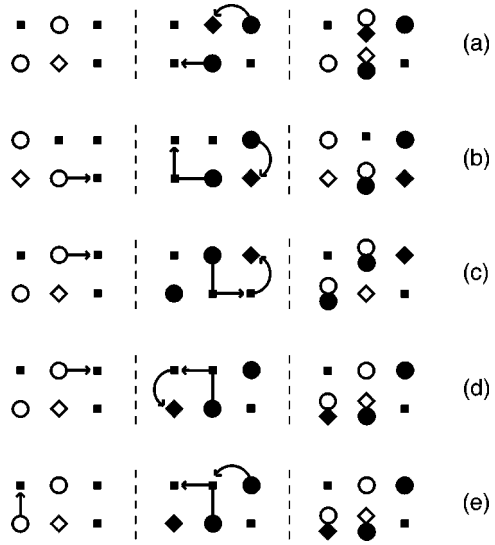

FIG. 10. Diagrammatic representation of some processes that contribute to the Hamiltonian matrix and are related to the kinetic part of the t-J model.

touch each other. We therefore have to make amendments in some elements of the Hamiltonian matrix H [see Fig. 9(a) for an example of such an amendment given by $-(J/2)\Sigma_{\mu=0,\nu=1}(z-1)^{\mu+\nu-1}\hat{\alpha}^2_{\mu,\nu}$].

In general, we restrict our considerations for contributions proportional to J to processes for which the total length of paths related to states coupled by those processes does not exceed two lattice spacings. Examples of all relevant types of processes related to the diagonal part of the Hamiltonian have been presented in Fig. 9. A process depicted by Fig. 9(b) is also related to an additional contribution to the over-

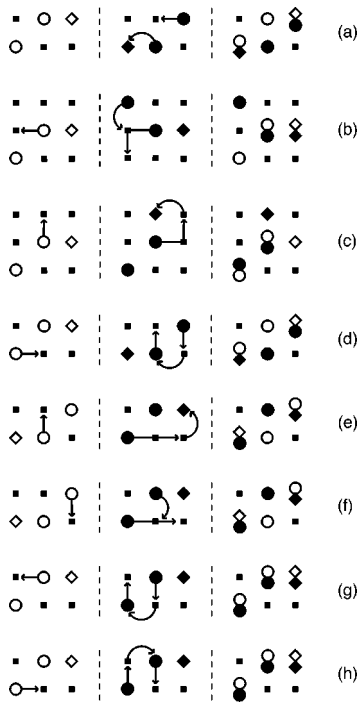

FIG. 11. Some processes that couple states $|\Phi^{(1)}_{l;\pm\hat{\mathbf{x}},\pm\hat{\mathbf{y}}}\rangle$ and $|\Phi^{(2)}_{l;\pm\hat{\mathbf{x}}\pm\hat{\mathbf{y}},\pm 2\hat{\mathbf{x}}\pm\hat{\mathbf{y}}(\pm\hat{\mathbf{x}}\pm 2\hat{\mathbf{y}})}\rangle$ and involve the kinetic term in the Hamiltonian.

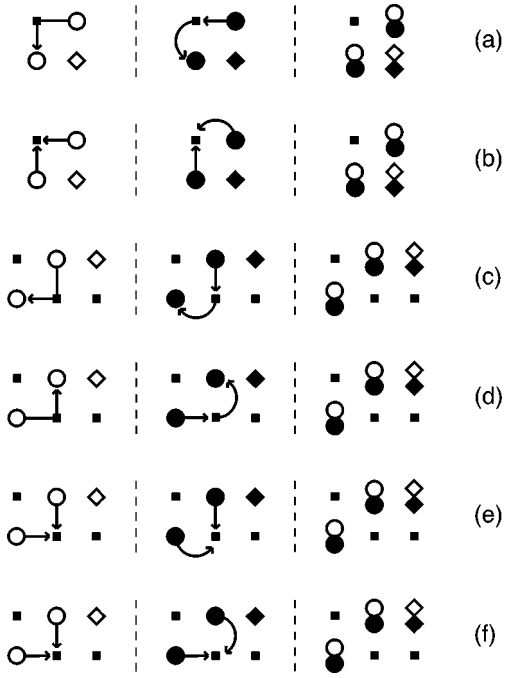

FIG. 12. Some spurious processes related to the hopping term in the Hamiltonian.

lap matrix. It is analogous to a process depicted by Fig. 6(a), and therefore has not been shown in Fig. 6. Figures 10 and 11 depict examples of processes that are related to the kinetic part of the Hamiltonian and give rise to some contributions to the Hamiltonian matrix. In our considerations we have taken account of all paths the length of which does not exceed two lattice spacings. Many processes that are analogous to those in Figs. 10 and 11 have not been shown because they are ruled by identical mechanisms and the only difference is their geometry.

The diagram in Fig. 10(a) gives rise to a contribution $t\Sigma_{\mu=0}(z-1)^{\mu}\hat{\alpha}_{\mu,0}\hat{\alpha}_{0,\mu+1}$ to an element that couples states $|\Phi^{(1)}_{i,-\hat{\mathbf{x}},\hat{\mathbf{y}}}\rangle$ and $|\Phi^{(1)}_{j,\hat{\mathbf{x}},-\hat{\mathbf{y}}}\rangle$, where $\mathbf{R}_j-\mathbf{R}_i=\hat{\mathbf{y}}$. A matrix element

$$t((z-1)^{-1}\tilde{\alpha}_0\hat{\alpha}_0\tilde{\alpha}_1\hat{\alpha}_0 + (z-2)\sum_{\mu=0}(z-1)^{\mu-1}\tilde{\alpha}_0\hat{\alpha}_1\tilde{\alpha}_{\mu+1}\hat{\alpha}_0),$$

which couples states $|\Phi^{(2)}_{i,\hat{\mathbf{x}}+\hat{\mathbf{y}},2\hat{\mathbf{x}}+\hat{\mathbf{y}}}\rangle$ and $|\Phi^{(2)}_{j,-\hat{\mathbf{x}}-\hat{\mathbf{y}},-2\hat{\mathbf{x}}-\hat{\mathbf{y}}}\rangle$, where $\mathbf{R}_j-\mathbf{R}_i=2\hat{\mathbf{x}}+\hat{\mathbf{y}}$, originates from a diagram in Fig. 11(a). Figure 12 depicts spurious processes related to the hopping term in the Hamiltonian, which are included in the Schrödinger equations (A3) and (A5) for $\hat{\alpha}$. Their contributions should be subtracted. A diagram in Fig. 12(a) gives rise to an amendment $t\hat{\alpha}_{0,2}\hat{\alpha}_{0,1}$ in a diagonal matrix element for a state $|\Phi^{(1)}_{l,-\hat{\mathbf{x}},\hat{\mathbf{y}}}\rangle$. Figures 13, 14, and 15 depict some processes that involve the exchange part of the Hamiltonian. Processes shown in Fig. 15 are specific to the 4×4 cluster, because they are related to periodic boundary conditions. A contribution $-(J/2)\Sigma_{\mu=0,\nu=2}(z-1)^{\mu+\nu-2}\hat{\alpha}_{\mu,\nu}\hat{\alpha}_{\mu,\nu-2}$ to a matrix element that couples states $|\Phi^{(1)}_{i,\hat{\mathbf{x}},\hat{\mathbf{y}}}\rangle$ and $|\Phi^{(1)}_{j,\hat{\mathbf{x}},\hat{\mathbf{y}}}\rangle$, where $\mathbf{R}_j-\mathbf{R}_i=\hat{\mathbf{x}}$, originates from a diagram in Fig. 13(b).

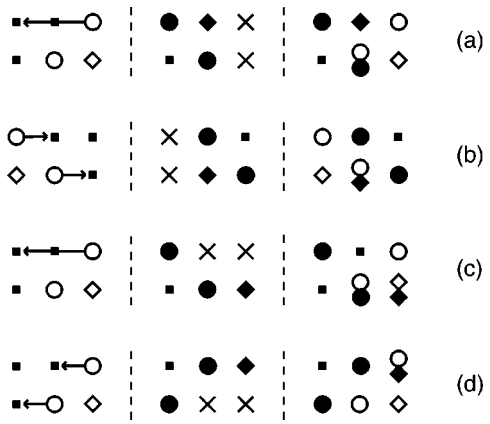

FIG. 13. Diagrammatic representation of some processes mediated by the exchange part of the Hamiltonian.

The diagram in Fig. 14(a) gives rise to a contribution

$$-(J/2)\Big[(z-1)^{-1}\tilde{\alpha}_2\hat{\alpha}_0\hat{\alpha}_{0,0}+(z-2)\times\sum_{\mu=2,\nu=0}(z-1)^{\mu+\nu-3}\tilde{\alpha}_\mu\hat{\alpha}_\nu\hat{\alpha}_{\nu,\mu-2}\Big]$$

to a matrix element that couples states $|\Phi^{(2)}_{i,\hat{\mathbf{x}}+\hat{\mathbf{y}},2\hat{\mathbf{x}}+\hat{\mathbf{y}}}\rangle$ and $|\Phi^{(1)}_{j,-\hat{\mathbf{x}},-\hat{\mathbf{y}}}\rangle$, where $\mathbf{R}_j-\mathbf{R}_i=2\hat{\mathbf{x}}+\hat{\mathbf{y}}$.

A contribution

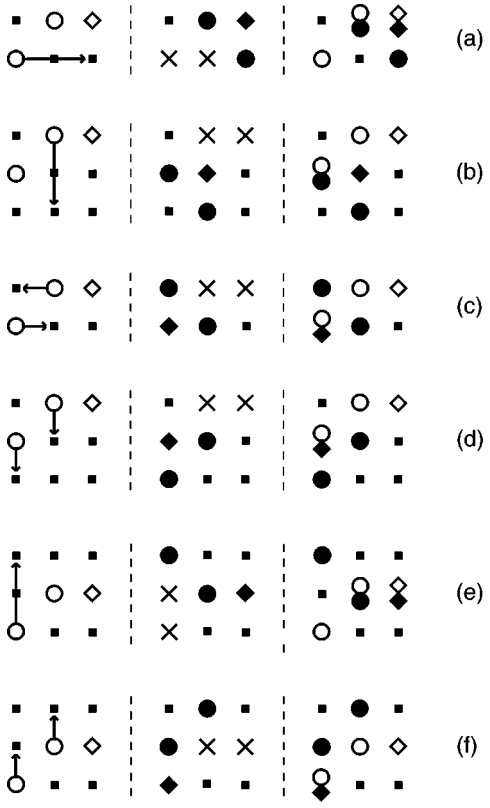

FIG. 14. Some processes mediated by the exchange part of the Hamiltonian that couple states $|\Phi^{(1)}_{l;\pm\hat{\mathbf{x}},\pm\hat{\mathbf{y}}}\rangle$ and $|\Phi^{(2)}_{l;\pm\hat{\mathbf{x}}\pm\hat{\mathbf{y}},\pm2\hat{\mathbf{x}}\pm\hat{\mathbf{y}}(\pm\hat{\mathbf{x}}\pm2\hat{\mathbf{y}})}\rangle$.

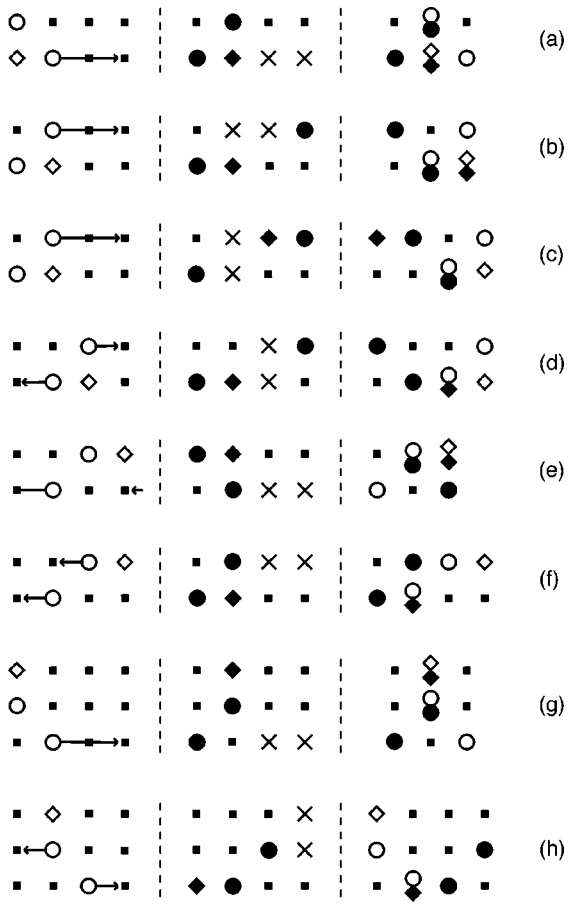

FIG. 15. Some processes mediated by the exchange part of the Heisenberg model that contribute to the Hamiltonian matrix and involve periodic boundary conditions.

$$(J/2)\Big[(z-1)^{-1}\hat{\alpha}_{2,0}\hat{\alpha}_{0,0}+(z-2)\times\sum_{\mu=2,\nu=0}(z-1)^{\mu+\nu-3}\hat{\alpha}_{\mu,\nu}\hat{\alpha}_{\mu-2,\nu}\Big]$$

to a matrix element coupling states $|\Phi^{(1)}_{l,\hat{\mathbf{x}},\hat{\mathbf{y}}}\rangle$ and $|\Phi^{(1)}_{l,-\hat{\mathbf{x}},\hat{\mathbf{y}}}\rangle$ is related to a diagram in Fig. 15(a).

Figures 3–15 do not contain all 117 processes that we have considered. On the other hand, those figures represent all mechanisms that govern processes involving paths of length not exceeding two lattice spacings. In the case of corrections to the diagonal contribution to eigenenergy we have restricted calculations to paths of length not exceeding one lattice spacing. Each diagram for 117 processes represents a contribution not only to matrix elements which couple states represented by the right part of that diagram, but also to all matrix elements which couple states obtained by action of lattice symmetry transformations.

V. COMPARISON BETWEEN VARIATIONAL APPROACH AND EXACT DIAGONALIZATION

Using the Lanczos algorithm we have calculated the lowest state for all the different space group representations. We

TABLE III. The energy difference between two and no hole states E_2-E_0; **k** is the total momentum, Rep. denotes the appropriate representation, $t=1$, $J=1/4$, spin bag wave functions were calculated for maximal string length of 5 lattice spacings. Figures in parentheses denote values obtained by means of the variational approach.

	A_1	A_2	B_1	B_2	E
(0,0)	−3.72 (−3.74)	−3.55 (−3.48)	−4.00 (−3.90)	−3.42 (−3.56)	−3.76 (−3.93)
(π,π)	−3.31 (−3.74)	−3.66 (−3.48)	−3.81 (−3.90)	−3.52 (−3.56)	−3.81 (−3.93)
$(\pi,0)$	−3.66 (−3.60)	−3.80 (−3.73)	−4.00 (−3.90)	−3.81 (−3.90)	
$(\pi/2,\pi/2)$	−3.79 (−3.60)	−3.81 (−3.93)			
$(\pi/2,0)$	−3.73 (−3.85)	−3.77 (−3.85)			
$(\pi,\pi/2)$	−3.77 (−3.85)	−3.73 (−3.85)			

have then repeated that task by means of the variational approach based on the string picture. In the latter case we have applied the trial wave functions that have been gathered in Tables I and II. Binding of holes appears for sufficiently large J/t ($\geqslant 0.27$).[20–22] We have therefore performed calculations for two values of J/t just near the critical ratio for $J/t=0.25$ and deep in the binding region for $J/t=0.5$. The region between those values seems to be very interesting also from the experimental viewpoint and most numerical studies indicate that those values are low enough to prevent phase separation.[23,24] The variational approach is based on a simplifying assumption, but in general not necessary, that the spin background is an ideal antiferromagnet. The spin bag scenario is also true for finite range antiferromagnetic correlations provided that they extend for a sufficiently long distance. In such a case a tendency towards localization of holes and towards formation of spin polarons determines the dynamics of holes. Correlations in a finite cluster are by definition not of infinite range. Two holes in a 16-site cluster mean a substantial amount of doping that reduces antiferromagnetic correlations.

The binding energy for the lowest state has been already calculated by means of the variational approach and presented in a paper by Wróbel and Eder[16] (see Figs. 18 and 21). In the present paper we concentrate on the issue of competition between states of different symmetry or importance of different precess and therefore use the energy of the Néel state as a point of reference. In Tables III and IV we present a comparison between structures of eigenenergies obtained by means of the variational approach based on the string picture and by means of an exact diagonalization. The essential difference between results of both calculations is that the energies for momenta that differ by (π,π) are not equal in the case of the exact diagonalization. All such states are by definition equivalent in the case of the variational approach because the assumption that spins in the background are arranged according to the Néel pattern induces a reduction in the size of the Brilloin zone. Two antiparallel Néel states on a cluster with an even number of N sites are coupled be a finite power of the Hamiltonian $H^{N/2}$ and their effective hybridization, which is neglected in the variational calculation, comes into play. But, on the other hand, the variational approach gives correctly the scale of the difference in energies of the two-hole state and the equivalent undoped system. It also selects the same group of states with small energy as the exact diagonalization. Those states are A_2 for $\mathbf{k}=(\pi/2,\pi/2)$, B_1 for $\mathbf{k}=0,(\pi,\pi),(\pi,0)$ and E for $\mathbf{k}=(\pi,\pi)$. The system chooses the ground state from that set of states. The value of the energy of the representation E is too low in the variational calculation, probably because cou-

TABLE IV. The energy difference between two and no hole states E_2-E_0; **k** is the total momentum, Rep. denotes the appropriate representation, $t=1$, $J=1/2$, spin bag wave functions were calculated for maximal string length of 5 lattice spacings. Figures in parentheses denote values obtained by means of the variational approach.

	A_1	A_2	B_1	B_2	E
(0,0)	−1.49 (−1.33)	−1.61 (−1.09)	−2.37 (−1.96)	−1.33 (−1.07)	−1.92 (−1.95)
(π,π)	−1.33 (−1.33)	−1.58 (−1.09)	−2.02 (−1.96)	−1.22 (−1.07)	−2.13 (−1.95)
$(\pi,0)$	−1.52 (−1.32)	−2.01 (−1.50)	−2.37 (−1.96)	−2.02 (−1.96)	
$(\pi/2,\pi/2)$	−2.01 (−1.32)	−2.13 (−1.95)			
$(\pi/2,0)$	−2.02 (−1.81)	−1.98 (−1.81)			
$(\pi,\pi/2)$	−1.98 (−1.81)	−2.02 (−1.81)			

pling between antiparallel Néel arrangements has been neglected. How important that coupling is may be seen in the case of the difference between energies for states A_1 or B_1 and $\mathbf{k}=0$ or $\mathbf{k}=(\pi,\pi)$.

The variational approach reproduces with some exceptions the structure of states for all momenta. As we have mentioned above, the main exception is the difference between energies corresponding to different representations for $\mathbf{k}=0$ and (π,π). The hierarchy of states for $\mathbf{k}=0$ is reproduced by the analytical approach with the exception of the E representation for $J/t=1/4$ and the A_2 representation for $J/t=1/2$. A state that transforms according to the E representation for $\mathbf{k}=0$ is the overall ground state for $J/t=1/4$ in the analytical calculation, but its energy is only slightly lower than the energy of the B_1 state, which is the true ground state of the cluster. In the case of $\mathbf{k}=(\pi,\pi)$, which is equivalent to the case $\mathbf{k}=0$ for the variational approach, we see that true energies for B_1 and E states are indeed near in value for $J/t=1/4$ and the energy of the E state for $J/t=1/2$ is lower than the energy of the B_1 state.

It is rather surprising why the true energy of the A_2 state is lower than energy of the A_1 state for $J/t=1/2$. The A_1 representation involves fully symmetric spin bag states while the A_2 representation consists of less symmetric spin bag states. It has been shown by Belinicher and co-workers[25] that inclusion of longer-range spin wave exchange can lower an A_2 (or g-wave) state sufficiently, so that it can compete with the B_1 state as the ground state. This state, however, is quite different from the present one, which is indeed a rather highly excited state. In the next section we present a simple explanation for the structure of states for intermediate values of J/t, which is based on the symmetry of the spin bag states and a few simple processes. That explanation sheds some light on the puzzle of the A_2 state.

The structure of states for $\mathbf{k}=(\pi,0)$ is preserved in the variational approach for $J/t=1/4,1/2$. The only inconsistency is that the two lowest states B_1 and B_2 are degenerate due to equivalence of states with momenta that differ by (π,π). The order of the states with $\mathbf{k}=(\pi/2,\pi/2)$ is the same in the case of the variational method as in the case of the exact diagonalization. All four states for $\mathbf{k}=(\pi/2,0),(\pi,\pi/2)$ are degenerate in the variational approach. The different representations A_1 and A_2 for different momenta are degenerate due to the equivalence of the 4×4 cluster and the 2^4 supercube, while the same representations A_1 (A_2) also for different momenta are degenerate due to the equivalence of momenta $(\pi/2,0)$ and $(\pi,\pi/2)$. The true energies for $\mathbf{k}=(\pi/2,0),(\pi,\pi/2)$, while not being equal, are close in value.

VI. MECHANISM OF BINDING IN DOPED ANTIFERROMAGNETS

The hierarchy of states with $\mathbf{k}=0$ that correspond to different irreducible representations of C_{4v} may be interpreted in terms of a much more reduced Hilbert space that consists only of states that correspond to pairs of holes created in an antiferromagnetic background at nearest-neighbor sites. The role of such states grows with the ratio J/t. Although the rise in the magnetic contribution to energy related with creation of a pair of static holes is minimal if they occupy two

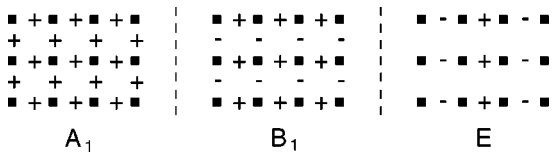

FIG. 16. Schematic representation of coherent sums of bipolaronic states $|\Phi^s_{i,\pm\hat{\mathbf{x}}(\pm\hat{\mathbf{y}})}\rangle$ that realize the representations A_1, B_1 and E for $\mathbf{k}=0$. A sign in the center of a bond represents a bipolaron that corresponds to two holes created at both ends of that bond.

nearest-neighbor sites, the kinetic contribution to energy grows in such a case because hopping of each hole in one direction is blocked by its companion. That loss may be compensated if holes follow each other in such a way that they jump on upturned spins left by the other hole. The motion of a pair of holes connected by a string seems to determine the properties of a bound state also for moderate values of J/t. We try to understand binding in terms of states that are coupled by processes corresponding to that type of motion. The reduced Hilbert space consists then of states $|\Phi^s_{i,\pm\hat{\mathbf{x}}(\pm\hat{\mathbf{y}})}\rangle$, where i belongs to the spin-up sublattice. The rich structure of the spin bag state $|\Phi^s_{i,\pm\hat{\mathbf{x}}(\pm\hat{\mathbf{y}})}\rangle$, which is a combination of many string states, may be represented by a single operator that corresponds to the creation of a spin bipolaron at sites $\mathbf{R}_i$ and $\mathbf{R}_j$, where $\mathbf{R}_j-\mathbf{R}_i=\pm\hat{\mathbf{x}}(\pm\hat{\mathbf{y}})$. Some coherent sums of bipolaronic states $|\Phi^s_{i,\pm\hat{\mathbf{x}}(\pm\hat{\mathbf{y}})}\rangle$ realize representations A_1, B_1, and E for $\mathbf{k}=0$. Figure 16 depicts schematically structure of those coherent combinations.

It is not possible to construct the representations A_2 and B_2 for $\mathbf{k}=0$ in terms of fully symmetric bipolaronic states $|\Phi^s_{i,\pm\hat{\mathbf{x}}(\pm\hat{\mathbf{y}})}\rangle$ and states which realize them must have higher energy than states which realize the representations A_1, B_1 and E. Bipolaronic states are combinations of states which may be obtained by consecutive hopping from a state which represents two holes created at nearest neighbor sites. They also may possess nontrivial internal symmetry. Bipolaronic states with a minimal loss of symmetry and a minimal rise in energy are combinations of states $|\Phi^{(1)}_{l,\pm\hat{\mathbf{x}}(\pm\hat{\mathbf{y}})}\rangle$. The states $|\Phi^{(2)}_{l;\pm\hat{\mathbf{x}}\pm\hat{\mathbf{y}},2\hat{\mathbf{x}}\pm\hat{\mathbf{y}}(2\hat{\mathbf{y}}\pm\hat{\mathbf{x}})}\rangle$ represent a combination of a fully symmetric polaron at a site i, and a polaron which has lower symmetry at a site j, where $\mathbf{R}_j-\mathbf{R}_i=2\hat{\mathbf{x}}\pm\hat{\mathbf{y}}(2\hat{\mathbf{y}}\pm\hat{\mathbf{x}})$. The static contribution to the energy from a component of $|\Phi^{(1)}_{i,\pm\hat{\mathbf{x}}(\pm\hat{\mathbf{y}})}\rangle$, which is a string state of shortest length (an upturned spin and two holes created at nearest-neighbor sites), is lower than the static contribution from a component of $|\Phi^{(2)}_{l;\pm\hat{\mathbf{x}}\pm\hat{\mathbf{y}},2\hat{\mathbf{x}}\pm\hat{\mathbf{y}}(2\hat{\mathbf{y}}\pm\hat{\mathbf{x}})}\rangle$ corresponding to a string state of shortest length, which is a combination of a hole and a single-hole string of length 1. The eigenenergy of $|\Phi^{(1)}_{l,\pm\hat{\mathbf{x}}(\pm\hat{\mathbf{y}})}\rangle$ should be therefore lower than the eigenenergy of $|\Phi^{(2)}_{l;\pm\hat{\mathbf{x}}\pm\hat{\mathbf{y}},2\hat{\mathbf{x}}\pm\hat{\mathbf{y}}(2\hat{\mathbf{y}}\pm\hat{\mathbf{x}})}\rangle$. A state that realizes the representation A_2 is a combination of states $|\Phi^{(1)}_{l,\pm\hat{\mathbf{x}}(\pm\hat{\mathbf{y}})}\rangle$ and $|\Phi^{(2)}_{l;\pm\hat{\mathbf{x}}\pm\hat{\mathbf{y}},2\hat{\mathbf{x}}\pm\hat{\mathbf{y}}(2\hat{\mathbf{y}}\pm\hat{\mathbf{x}})}\rangle$, while the representation B_2 is a combination only of states $|\Phi^{(2)}_{l;\pm\hat{\mathbf{x}}\pm\hat{\mathbf{y}},2\hat{\mathbf{x}}\pm\hat{\mathbf{y}}(2\hat{\mathbf{y}}\pm\hat{\mathbf{x}})}\rangle$. It is therefore clear that the A_2 state should have lower energy than the B_2 state. The dominant processes that involve the kinetic part of

TABLE V. Strength of different process which contribute to the overlap and the energy for representations A_1, B_1, and E. Figures in parentheses denote bare matrix elements.

Rep.	W_{bp}	W_{pp}	E_{bb}	E_{dif}	E_{cat}	E_{exbb}	E_{expp}	E_{exbp}
A_1	0.27(0.57)	0.73(4.0)	$-0.05(-0.11)$	0.00(0.00)	0.32(0.68)	0.16(0.33)	0.47(2.6)	$-0.97(-3.3)$
B_1	0.78(5.9)	0.22(4.0)	$-0.16(-1.2)$	0.00(0.01)	$-0.15(-1.1)$	$-0.14(-1.0)$	$-0.05(-0.86)$	$-0.09(-1.1)$
E	0.52(3.1)	0.48(2.0)	$-0.10(-0.60)$	0.00(0.01)	$-0.11(-0.66)$	$-0.01(-0.06)$	$-0.10(-0.43)$	$-0.22(1.1)$

the Hamiltonian and string states of shortest length are represented by Fig. 3(c). By counting states that are coupled by those processes with a certain bipolaronic state we conclude the the contribution to energy per bond occupied by a bipolaron is $6\tau_1$ for the representation A_1 and $-2\tau_1$ for the representations B_1 and E, where $\tau_1=t\tilde{\alpha}_{0,0}\tilde{\alpha}_{0,1}>0$ and therefore the A_1 state will have higher energy than the B_1 and E states. The positive sign of the contribution to energy for the representation A_1 which originates from that processes explains why the energy of the A_2 state is lower than the energy of the A_1 state for $J/t=0.5$. It turns out that the gain related to a higher symmetry of spin bag states that contribute to the A_1 state is compensated by contributions from processes represented by elements of the Hamiltonian matrix and related to the hopping term. Processes that involve longer strings should decide what symmetry, B_1 or E, possess the ground state for the two-hole problem in the t-J model. Processes that are represented by Fig. 3(d) are not conclusive because their contribution is $2\tau_2$ for both states B_1 and E, where $\tau_2=-t\Sigma_{\mu=0}(z-1)^{\mu}\tilde{\alpha}_{\mu,1}\tilde{\alpha}_{\mu+2,0}$. We proceed then to analysis of processes that involve the exchange part of the Hamiltonian. A contribution from processes depicted in Fig. 4(a) is $-8\theta_1$, where $\theta_1=(J/2)\Sigma_{\mu=0,\nu=2}(z-1)^{\mu+\nu-2}\tilde{\alpha}_{\mu,\nu}\tilde{\alpha}_{\mu,\nu-2}$, in the case of the B_1 representation and vanishes for the E representation. That favors the B_1 representation for the infinite lattice. In the case of the 4×4 cluster with periodic boundary conditions the process depicted by Fig. 5(a) neutralizes the contribution from the process represented by Fig. 4(a) (it gives rise to the contribution $4\theta_1$ to energy of the B_1 state and $-4\theta_1$ to energy of the E state). The contribution from the process depicted by Fig. 4(b) is $4\theta_2$ for both representations B_1 and E, where $\theta_2=-(J/2)\Sigma_{\mu=1,\nu=1}(z-1)^{\mu+\nu-2}\tilde{\alpha}_{\mu,\nu}\tilde{\alpha}_{\mu-1,\nu-1}$. The process depicted by Fig. 5(b) favors the B_1 representation. Its contribution to energy per bond occupied by a bipolaron is $2\theta_2$ for the B_1 state and $-2\theta_2$ for the E state. That process plays therefore the decisive role in the case of the 4×4 cluster with periodic boundary conditions.

In order to confront the heuristic way of reasoning with results obtained by means of the full version of the variational approach we have additionally calculated contributions to the energy from different processes for the representations A_1, B_1, E, ($\mathbf{k}=0$, $J/t=0.4$) and wave functions gathered in Table I. Table V contains results of that calculation. W_{bp} denotes the weight in the variational wave function of functions $|\Psi^{s}_{i,\pm\hat{\mathbf{x}}(\pm\hat{\mathbf{y}})}\rangle$ representing bipolarons. W_{pp} is the weight of functions $|\Psi^{s}_{i,2\hat{\mathbf{x}}\pm\hat{\mathbf{y}}(2\hat{\mathbf{y}}\pm\hat{\mathbf{x}})}\rangle$ representing pairs of spin polarons. E_{bb} denotes the gain in energy due to the fact that the diagonal contribution to energy [the term $J\Sigma_{\langle i,j\rangle}(S_{i,z}S_{j,z}-n_in_j/4)$] from states $|\Psi^{s}_{i,\pm\hat{\mathbf{x}}(\pm\hat{\mathbf{y}})}\rangle$ is lower because a pair of holes is created on nearest-neighbor sites (and one ''broken'' bond is saved). E_{dif} is a gain or a loss due to the difference between the eigenenergy of a bipolaron $\tilde{E}_2$ and eigenenergy of two polarons $2\tilde{E}_1$. It is defined as a product of a factor $\tilde{E}_2-2\tilde{E}_1-1/3J$ and the weight of the spin bipolaron in the variational wave function. The term $-1/3J$ in the first factor is related to a contribution from quantum fluctuations in the spin background. E_{cat} denotes the contribution to energy from processes shown in Figs. 3(c) and 3(d). They represent motion of two holes connected by a string of upturned spins that resembles motion of a caterpillar. E_{exbb} is the contribution to the energy from the exchange term $(J/2)\Sigma_{\langle i,j\rangle}(S_i^+S_j^-+S_i^-S_j^+)$ that is restricted to the wave functions $|\Psi^{s}_{i,\pm\hat{\mathbf{x}}(\pm\hat{\mathbf{y}})}\rangle$ representing spin bipolarons. E_{expp} denotes an analogous contribution related to pairs of bipolarons and states $|\Psi^{s}_{i,2\hat{\mathbf{x}}\pm\hat{\mathbf{y}}(2\hat{\mathbf{y}}\pm\hat{\mathbf{x}})}\rangle$. E_{exbp} is that part of energy that originates from the exchange term and coupling between states representing spin bipolarons and pairs of spin polarons. Table V contains values of all quantities defined above. Figures in parentheses represent the absolute strength of each type of contribution and are explicitly related to elements of overlap and Hamiltonian matrices coupling components of variational wave functions representing spin bipolarons or pairs of polarons. Provided that the variational wave functions are normalized the numbers outside the parentheses may be obtained by multiplying those in parentheses by the products aa, bb or ab (defined in Table I). It is obvious that the additional variational analysis, the results of which are presented in Table V, confirms the heuristic line of reasoning that we discussed above. The bipolaronic state has largest weight in the bound state of B_1 symmetry. The B_1 and E states take advantage of the caterpillarlike motion of holes in the most efficient way. Processes related to the magnetic exchange that couple bipolaronic states favor the B_1 symmetry. The ''unbinding'' of a bipolaron into a pair of polarons is in favor of the states E and A_1, because such a pair takes advantage of the exchange interaction in a more efficient way. The latter observation may explain why the E state has lower energy than the B_1 state for $\mathbf{p}=(\pi,\pi)$, but we think that the role of processes of that type is overestimated by the variational approach. When comparing matrix elements related to different contributions to the energy one has to keep in mind that their relevance also depends on the overlap between states that they couple. Elements of the overlap matrix for the B_1 states are approximately two times bigger than those for the E_1 state. The effectiveness of matrix elements related to E_{bb}, E_{cat}, and E_{expp} is then similar for both representations. Processes that

contribute to E_{exbb} definitely favor the B_1 representation, while those which contribute to E_{exbp} are in favor of the E representation, despite the fact that in the later case the moduli of matrix elements (in parentheses) are approximately the same. An interesting observation is that the gain in energy due to smaller contribution from the diagonal part of the Hamiltonian to the eigenenergy of spin bipolarons (E_{bb}) is compensated by a loss of kinetic energy, which is due to the fact that holes cannot jump onto each other. A manifestation of that compensation is that the difference between the eigenenergy of the bipolaron and the eigenenergy of a pair of polarons vanishes almost exactly for $J/t=0.4$ ($E_{dif}\sim 0.0$). The decisive role in formation of the bound state B_1 which predominantly consists of the bipolaronic states is hopping of bipolarons, that is related to the caterpillarlike motion of hole pairs, and contributions to the energy related to the magnetic exchange.

The mechanism of hole binding thus is a relatively complex one, and the simple broken-bond argument, namely, that holes bind because a hole pair on nearest neighbors leaves intact one more exchange bond, is by no means adequate. Instead, for physical parameters, the broken-bond contribution is completely compensated by a loss of kinetic energy occurring at the same time, because two holes on nearest neighbors have only $2(z-1)$ nearest neighbors available for charge fluctuations (whereas it is $2z$ for separate holes). The actual binding mechanism is provided by the caterpillar-type motion of the two holes. Pair symmetries that get the most out of the caterpillar motion, i.e., B_1 and E, are lowest in energy, both at $(0,0)$ and (π,π).

VII. PAIR STRUCTURE

Some recent density matrix renormalization group[26] and exact diagonalization[27] studies of the two hole problem in small ladders and two-dimensional clusters concern the spatial distribution of holes and spin correlations in their vicinity. Holes in planes are mainly located at distances 1, $\sqrt{2}$, and $\sqrt{5}$ lattice spacings from each other, while the probability that the distance between them is 2 turns out to be much smaller. Those studies also show that a strong spin singlet forms along the diagonal of a lattice cell if the holes occupy the sites belonging to the other diagonal. We are then tempted to check whether those findings can be explained by the spin bag scenario.

We restrict the calculation of the hole density-density correlation function to contributions from states $|\{(i,\mathcal{P}),\},\{\varnothing\}\rangle$ related to shortest strings. Figures 17(a)–17(g) depict different categories of diagrams which contribute to the probability of finding two holes at two nearest-neighbor sites. The rest of relevant diagrams may be obtained by applying some symmetry transformations of the lattice. Two different string states that belong to the category represented by Fig. 17(b) and a string state depicted by Fig. 17(c) give rise to the same configuration of holes and spins. The absolute value of the amplitude for that state is the sum of the absolute values of amplitudes for all three string states. Two string states related to Fig. 17(b) contribute with a negative sign, because spin bag states $|\Phi^{s}_{i,\hat{\mathbf{y}}}\rangle$ and $|\Phi^{s}_{i,-\hat{\mathbf{y}}}\rangle$ also contribute with a negative sign to the wave function that transforms according to the B_1 representation for $\mathbf{k}=0$. The contribution from the string state represented by Fig. 17(c) is also negative because of the Fermi statistics and the fact that holes change the sublattices. The final state consists of two holes that occupy the sites i_1 and j_1 and two upturned spins at the sites i_2 and j_2. A negative sign and amplification of its amplitude, which reads $-a(\tilde{\alpha}_{1,1}+2\tilde{\alpha}_{0,2})$, actually stems from the d-wave symmetry of the ground state. The amplitude of a state represented by Fig. 17(a) is $a\tilde{\alpha}_{0,0}$. That state simultaneously contributes to the spin singlet or triplet at the sites i_2, j_2. Due to the different signs of amplitudes for states represented by Fig. 17(a) and by Figs. 17(b) and 17(c), the weight of the singlet is amplified. The diagrams represented by Figs. 17(d)–17(g) give rise to different hole and spin configurations and therefore they contribute individually to to the probability of finding holes at two different sites. Some of them may favor the spin triplet like Fig. 17(d), which represents a configuration with parallel spins at the sites i_2 and j_2. The rest of the diagrams contribute to the same extent to the singlet and the triplet. Provided that the B_1 state in Table I is normalized, the probability of finding holes at the distance of one lattice spacing from each other reads

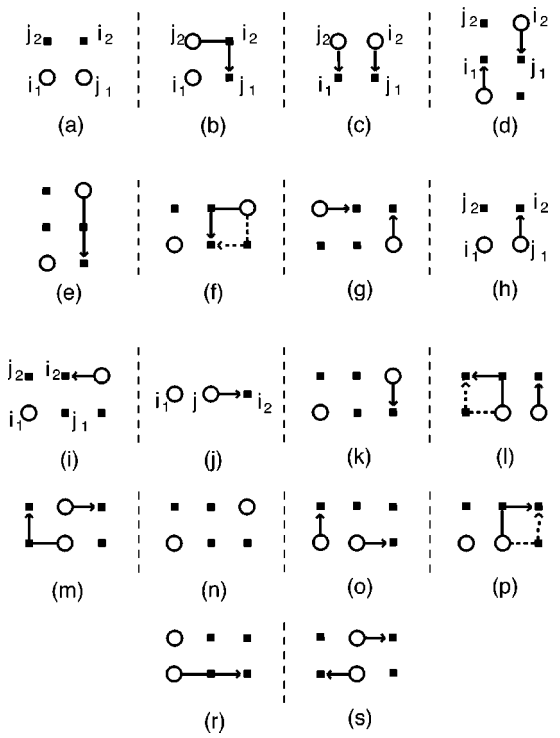

FIG. 17. Simplest string states contributing to the hole density-density correlation function for short distances.

$$P(1)=4\{a^2[\tilde{\alpha}_{0,0}^2+2(2\tilde{\alpha}_{0,2}+\tilde{\alpha}_{1,1})^2]+b^2(6\tilde{\alpha}_1^4+12\tilde{\alpha}_0^2\tilde{\alpha}_2^2)\}, \tag{13}$$

while the weight of the spin singlet at the second pair of corners of the lattice cell is given by

$$P_s(1)=\frac{a^2\left[\frac{(\tilde{\alpha}_{0,0}+2\tilde{\alpha}_{0,2}+\tilde{\alpha}_{1,1})^2}{2}+\frac{(2\tilde{\alpha}_{0,2}+\tilde{\alpha}_{1,1})^2}{2}\right]+b^2(\tilde{\alpha}_1^4+4\tilde{\alpha}_0^2\tilde{\alpha}_2^2)}{a^2[\tilde{\alpha}_{0,0}^2+2(2\tilde{\alpha}_{0,2}+\tilde{\alpha}_{1,1})^2]+b^2(6\tilde{\alpha}_1^4+12\tilde{\alpha}_0^2\tilde{\alpha}_2^2)}. \quad (14)$$

We have calculated both quantities for $J/t=0.4$ and obtained $P(1)\simeq 0.16$ and $P_s(1)=0.7$. A calculation for contributions from the shortest strings to the hole density-density correlation function for sites at ends of an elementary cell diagonal is much simpler. Figures 17(h) and 17(i) depict two relevant sets of diagrams that represent strings of length 1. Contributions from four diagrams obtained from Fig. 17(h) by transformations that keep the pair of the sites i_1 and i_2 unchanged constitute a perfect spin singlet at the sites j_1 and j_2. That reason for the preference for the spin singlet along a cell diagonal has been noticed by Riera and Dagotto.[27] It follows from the *d*-wave symmetry of the ground state and the existence of antiferromagnetic correlations. But, on the other hand, for similar reasons, contributions from all four diagrams analogous to Fig. 17(i) amplify the weigh of the spin triplet. It is therefore an issue of numerical assessment which tendency prevails. The contribution from diagrams represented by Figs. 17(h) and 17(i) to the probability that the distance between holes is $\sqrt{2}$ reads

$$P(\sqrt{2})=4(a^2 8\tilde{\alpha}_{0,1}^2+b^2 4\tilde{\alpha}_0^2\tilde{\alpha}_1^2), \quad (15)$$

while the weight of the spin singlet at the ends of a cell diagonal in the case of holes occupying the ends of the second diagonal is

$$P_s(\sqrt{2})=\frac{a^2 2\tilde{\alpha}_{0,1}^2}{a^2 2\tilde{\alpha}_{0,1}^2+b^2\tilde{\alpha}_0^2\tilde{\alpha}_1^2}. \quad (16)$$

Numerical calculation for $J/t=0.4$ gives $P(\sqrt{2})=0.18$ and $P_s(\sqrt{2})=0.8$. Exact diagonalization studies also indicate that the probability of finding holes at the distance 2 lattice spacings between each other, $P(2)$ is much lower than probabilities for the distances 1, $\sqrt{2}$, and $\sqrt{5}$. There is, as we are going to demonstrate, a very close relation between the $d_{x^2-y^2}$ symmetry of the bound state, antiferromagnetic correlations, and that phenomenon. Figures 17(j) and 17(k) depict categories of diagrams that might contribute to $P(2)$ and represent strings of length 1. A contribution from Fig. 17(j) (a string state that is a component of $|\Phi^s_{i_1,\hat{\mathbf{x}}}\rangle$) cancels a contribution from an analogous diagram that may be obtained by exchanging the sites i_1 and i_2 (a string, that is a component of $|\Phi^s_{i_2,-\hat{\mathbf{x}}}\rangle$). That cancellation is exact due to the structure of the B_1 state and the fact that a hole that starts at the site *j* moves to the different sublattice either to the site i_1 or to the site i_2. A contribution to $P(2)$ from states $|\Phi^s_{i,\pm\hat{\mathbf{x}}(\pm\hat{\mathbf{y}})}\rangle$ is then related to longer strings and may be smaller than in the case of distances 1, $\sqrt{2}$, and $\sqrt{5}$. Figures 17(l) and 17(m) represent contributions to $P(2)$ related to strings of total length 3. A straightforward calculation gives rise to a conclusion that

$$P(2)=a^2 64(\tilde{\alpha}_{1,2}+\tilde{\alpha}_{0,3})^2+b^2 16\tilde{\alpha}_0^2\tilde{\alpha}_2^2. \quad (17)$$

For $J/t=0.4$ we get $P(2)\simeq 0.09$. Figures 17(n)–17(s) represent contributions to $P(\sqrt{5})$ related to the shortest strings. They give

$$P(\sqrt{5})=a^2[16\tilde{\alpha}_{1,1}^2+8(\tilde{\alpha}_{1,1}+2\tilde{\alpha}_{0,2})^2]+b^2 4\tilde{\alpha}_0^4 \quad (18)$$

and $P(\sqrt{5})=0.16$ for $J/4=0.4$ The distribution of probability for finding holes at different distances obtained by means of the variational approach qualitatively agrees with results of the exact diagonalization reported by Riera and Dagotto for $J/t=0.4$ and slightly larger clusters.[27] The probability of finding holes at ends of a cell diagonal is highest, but distances 1 and $\sqrt{5}$ are also privileged. Holes do not predominantly occupy nearest-neighbor sites because owing to that, the optimal balance between kinetic and magnetic contributions to the energy may be reached. We also observe that effect in numerical solutions of the Schrödinger equation for $\tilde{\alpha}_{\mu,\nu}$. The probability of finding holes at the distance of 2 lattice spacings from each other is lower because contributions from some diagrams cancel due to the *d*-wave symmetry of the ground state. The numerical values of probabilities obtained in our calculation are lower than those obtained by means of exact diagonalization because we have neglected contributions from longer strings. It seems, on the other hand, that the role of short strings is underestimated in our approach.

VIII. DISCUSSION

In considering two hole ground states for all representations of small groups for the square lattice, in the case of the 4×4 cluster, we have found qualitative agreement between the exact diagonalization and the variational approach based on the string picture. We have constructed polaronic states representing a hole or a pair of holes trapped in a region in which the antiferromagnetic spin structure is strongly perturbed. Spin polarons (bipolarons) may propagate without disrupting the spin background more than necessary. We have taken into account in our calculation a list of more than 100 processes that induce a perturbation in the spin structure on no more than two sites. Such processes give rise to overlap and coupling between polaronic states. An important category of processes that contribute to coupling may be visualized as motion of a string of defects (upturned spins), spanning a sequence of nearest-neighbor sites between two holes. The ends of a string hop between nearest-neighbor sites in such a way that its length does not exceed a few lattice spacings. The next important class of processes is related to the exchange term, which may flip two antiparallel spins in nearest-neighbor sites and in that way may remove defects from the spin arrangement. Spin polaron or equivalently spin bag states may have nontrivial symmetry. Lower-

ing the symmetry of spin bag states raises their eigenenergy. The majority of representations may be realized in terms of fully symmetric spin polaron states, but the rest involves nontrivial states. The variational approach reproduces the basic features of the structure of states. It selects the correct group of low-energy states and for $\mathbf{k}=0,(\pi,\pi)$ points to competition between the representations B_1 and E for the position of the ground state. A qualitative explanation for $\mathbf{k}=0$ based on the symmetry of spin polaron states and a few important processes demonstrates why the system selects the representation B_1 as a ground state. The agreement between the spin bag approach and the exact diagonalization is also satisfactory for momenta $(\pi,0)$, $(\pi/2,\pi/2)$, $(\pi/2,0)$, and $(\pi,\pi/2)$. The variational calculation reproduces with semiquantitative precision the change in scale of the energy of two-hole states. The exact diagonalization performed in a 20-site cluster with periodic boundary conditions by Riera and Dagotto[27] indicates that a strong singlet is present across two sites that are diagonally situated in a plaquette, provided that two holes occupy the other two sites. These authors pointed out that such finding is consistent with the *d*-wave symmetry of the pair and antiferromagnetic correlations. Our calculation which also takes into account states preferring the triplet agrees with results of their exact diagonalization. The same conclusion concerns the spin singlet on a pair of nearest-neighbor sites, when the other two corners of the plaquette are occupied by holes. The diagonalization by Riera and Dagotto indicates that the density of a hole is spread over the neighborhood of the second hole. It is remarkable that the probability of finding holes at the distance of two lattice spacings between each other is much smaller than for 1, $\sqrt{2}$, and $\sqrt{5}$ lattice spacings. Our calculation demonstrates that this preference is consistent with the spin bag scenario. It seems that an important drawback of our variational approach is that for two holes it underestimates the role of states related to short strings. In order to deal with that problem we have restricted their length to five lattice spacings.

Some attempts have been made to describe the *t*-*J* model in terms of an effective Hamiltonian that contains only one interaction term representing attraction between quasiparticles on nearest-neighbor sites.[12] The origin of that attraction was attributed to reduction of the static diagonal contribution to the energy in the case of two holes occupying nearest-neighbor sites. The quasiparticles then should have much in common with bare holes. The two particles may not be located across the diagonals of a plaquette for the $d_{x^2-y^2}$ symmetry to be realized. Numerical studies have shown that such configuration of holes has a substantial weight in the ground state[21] and therefore a description of a weakly doped *t*-*J* model in terms of an oversimplified effective model in not possible. Spin excitations of bosonic character related to upturned spins are apparently important if antiferromagnetic correlations at short distances are robust. They have a finite lifetime and therefore induce retardation effects in the iterations between holes.[27] There can be no question that an effective Hamiltonian for weakly doped antiferromagnets should either deal explicitly with bosonic degrees of freedom or change the nature of quasiparticles and put the polaronic complexion on them. We have chosen the second way based on the spin bag scenario in order to get rid of bosonic degrees of freedom and incorporate complicate processes that involve spin excitations and contribute to interaction between polarons. The variational approach turned out to be a very powerful for implementation of that program, because it incorporates the relevant part of the interaction and is valid even in the case of short-range antiferromagnetic correlations. In agreement with results of Belinicher and co-workers[25] our calculations show that the broken-bond mechanism is not the driving force for hole pairing.

Our results for the one-dimensional *t*-*J* model in a staggered magnetic field[17] suggest, like some previous analyses[23], that phase separation in not very likely at low or intermediate J/t and low doping. Some experiments have demonstrated the existence of an ordered stripe phase in the cuprates.[28] Such a phase in the shape of domain walls of holes separating antiferromagnetically ordered domains might exist in the *t*-*J* model for certain values of doping concentration. One can imagine ''tunneling'' of holes through antiferromagnetic domains, which should be governed by the same processes as hole propagation in the antiferromagnetic medium. Provided the the structure of the stripe phase is known, the string picture might then contribute to a better understanding of fermionlike excitations in that phase.

ACKNOWLEDGMENTS

Support of P.W. by KBN under Project No. 2PO3B14612 is gratefully acknowledged.

APPENDIX A

The Schrödinger equation for spin polaron states $|\Psi_{\{i_k\},\{j_l\}}\rangle$ that represent holes trapped in the Néel state with some upturned spins takes the following form:

$$\frac{J}{2}\mathcal{L}(\{(i_k,\mathcal{P}_k)\},\{j_l\})\alpha_{\{(i_k,\mathcal{P}_k)\},\{j_l\}} - t\sum_{(i_k,\mathcal{P}'_k)\in\mathcal{T}(\{(i_k,\mathcal{P}_k)\},\{j_l\})}\alpha_{\{(i_k,\mathcal{P}'_k)\},\{j_l\}} = E_{\{i_k\},\{j_l\}}\alpha_{\{(i_k,\mathcal{P}_k)\},\{j_l\}}, \tag{A1}$$

where $\mathcal{L}(\{(i_k,\mathcal{P}_k)\},\{j_l\})$ is the number of broken bonds between nearest-neighbor sites in a state $|\{(i_k,\mathcal{P}_k)\},\{j_l\}\rangle$ and $\mathcal{T}(\{(i_k,\mathcal{P}_k)\},\{j_l\})$ is a set of states $|\{(i_k,\mathcal{P}'_k)\},\{j_l\}\rangle$ that are coupled with the state $|\{(i_k,\mathcal{P}_k)\},\{j_l\}\rangle$ by the hopping term of the Hamiltonian. We define a bond as ''broken'' if spins at sites joined by it are parallel or if at least at one of those sites a hole has been created. First term in the left side of Eq. (A1) originates from the term $J\Sigma_{\langle i,j\rangle}(S_i^zS_j^z-n_in_j/4)$ in the Hamiltonian.

We may write, according to Eq. (A1) a Schrödinger equation for coefficients $\tilde{\alpha}_\mu$, which represent trapping of a single hole in an antiferromagnetic environment,

$$-zt\tilde{\alpha}_1+2J\tilde{\alpha}_0=\tilde{E}_1\tilde{\alpha}_0,$$

$$-t\tilde{\alpha}_{\mu-1}-(z-1)t\tilde{\alpha}_{\mu+1}+J(\tfrac{5}{2}+\mu)\tilde{\alpha}_\mu=\tilde{E}_1\tilde{\alpha}_\mu, \tag{A2}$$

where $\mu \geq 1$. A Schrödinger equation for a hole trapped near a site with an upturned spin takes a similar form,

$$-t\hat{\alpha}_{\mu-1}-(z-1)t\hat{\alpha}_{\mu-1}+J(\tfrac{7}{2}+\mu)\hat{\alpha}_{\mu}=\hat{E}_1\hat{\alpha}_{\mu}, \quad \text{(A3)}$$

and $\hat{\alpha}_{\mu}=0$ for $\mu<0$.

Motion of two holes created at a pair of nearest neighbor sites is described by the following Schrödinger equation the form of which is again determined by the shape of a potential well of a spin bag,

$$-t[\tilde{\alpha}_{\mu-1,\nu}+(z-1)t\tilde{\alpha}_{\mu+1,\nu}+\tilde{\alpha}_{\mu,\nu-1}+(z-1)t\tilde{\alpha}_{\mu,\nu+1}] + J(4+\mu+\nu-\tfrac{1}{2}\delta_{\mu+\nu,0})\tilde{\alpha}_{\mu,\nu}=\tilde{E}_2\tilde{\alpha}_{\mu,\nu}, \quad \text{(A4)}$$

where $\tilde{\alpha}_{\mu,\nu}=0$ for $\mu<0$ or $\nu<0$.

A Schrödinger equation for two holes created at two different sites that are nearest neighbors of a site with an upturned spin is defined as

$$-t[\hat{\alpha}_{\mu-1,\nu}+(z-1)t\hat{\alpha}_{\mu+1,\nu}+\hat{\alpha}_{\mu,\nu-1}+(z-1)t\hat{\alpha}_{\mu,\nu+1}] + J(5+\mu+\nu)\hat{\alpha}_{\mu,\nu}=\hat{E}_2\hat{\alpha}_{\mu,\nu}, \quad \text{(A5)}$$

where $\hat{\alpha}_{\mu,\nu}=0$ for $\mu<0$ or $\nu<0$.

States $|\Phi^{s}_{i,\pm\hat{\mathbf{x}}(\pm\hat{\mathbf{y}})}\rangle$, $|\Phi^{s}_{i,\pm 2\hat{\mathbf{x}}\pm\hat{\mathbf{y}}(\pm 2\hat{\mathbf{y}}\pm\hat{\mathbf{x}})}\rangle$, $|\Phi^{(1)}_{l;\pm\hat{\mathbf{x}},\pm\hat{\mathbf{y}}}\rangle$, and $|\Phi^{(2)}_{l;\pm\hat{\mathbf{x}}\pm\hat{\mathbf{y}},\pm 2\hat{\mathbf{x}}\pm\hat{\mathbf{y}}(\pm\hat{\mathbf{x}}\pm 2\hat{\mathbf{y}})}\rangle$ are normalized provided that coefficients $\tilde{\alpha}$ and $\hat{\alpha}$ are subject to some additional conditions,

$$\tilde{\alpha}_0^2+\sum_{\mu=1}^{\infty} z(z-1)^{\mu-1}\tilde{\alpha}_{\mu}^2=1, \quad \text{(A6)}$$

$$\sum_{\mu=0}^{\infty}(z-1)^{\mu}\hat{\alpha}_{\mu}^2=1, \quad \text{(A7)}$$

$$\sum_{\mu=0,\nu=0}^{\infty}(z-1)^{\mu+\nu}\tilde{\alpha}_{\mu,\nu}^2=1, \quad \text{(A8)}$$

$$\sum_{\mu=0,\nu=0}^{\infty}(z-1)^{\mu+\nu}\hat{\alpha}_{\mu,\nu}^2=1. \quad \text{(A9)}$$

By choosing the Néel state to play the role of the antiferromagnetic environment for holes we have neglected spin fluctuations that exist in the ground state of the Heisenberg model. Quantum fluctuations produced by the transverse part of the Hamiltonian are responsible for lowering of the ground-state energy of the Heisenberg model in comparison with the ground-state energy of the Ising model. One can easily understand origin of that lowering by means of the second-order perturbation theory that attributes the reduction of energy by $J/12$ to presence of a quantum fluctuation in the form of two upturned spins on a pair of nearest-neighbor sites. Existence of a hole at a site prohibits creation of such fluctuations at four bonds attached to that site and raises energy by $4\times J/12$ in comparison with the ground state of the Heisenberg model. A quantum fluctuation in the spin background for spin bag states might give rise to additional overlap between them. Let us suppose, for example, that two slanted crosses in the central part of Fig. 4(a) represent a quantum fluctuation in the spin background for the state $|\Phi^{s}_{i,\hat{\mathbf{y}}}\rangle$. A configuration of holes and spins that correspond to the central part of Fig. 4(a) is identical to a string state that is a component of the state $|\Phi^{s}_{i,\hat{\mathbf{x}}}\rangle$ [the left part of Fig. 4(a)]. It turns out that such a type of overlap may wreck linear independence of spin bag states. We make therefore an assumption that quantum fluctuations are prohibited at sites that are nearest neighbors of sites where holes have been originally created. Any part of the Hilbert space is not neglected in our consideration because the same configuration of holes and spins is realized as a different string state, as in the case of the left and central parts of Fig. 4(a). Some fluctuations in the spin background are nevertheless prohibited and energy is raised in comparison with the ground state of the Heisenberg model. In all calculations we have therefore to make following substitutions in order to take into account the contribution from quantum fluctuations in the spin background:

$$|\Phi^{s}_{i,\pm\hat{\mathbf{x}}(\pm\hat{\mathbf{y}})}\rangle: \quad \tilde{E}_2\rightarrow\tilde{E}_2+\frac{22}{12}J, \quad \text{(A10)}$$

$$|\Phi^{s}_{l,2\hat{\mathbf{x}}\pm\hat{\mathbf{y}}(2\hat{\mathbf{y}}\pm\hat{\mathbf{x}})}\rangle: \quad 2\tilde{E}_1\rightarrow 2\tilde{E}_1+\frac{26}{12}J, \quad \text{(A11)}$$

$$|\Phi^{(1)}_{l;\pm\hat{\mathbf{x}},\pm\hat{\mathbf{y}}}\rangle: \quad \hat{E}_2\rightarrow\hat{E}_2+\frac{24}{12}J, \quad \text{(A12)}$$

$$|\Phi^{(2)}_{l;\pm\hat{\mathbf{x}}\pm\hat{\mathbf{y}},\pm 2\hat{\mathbf{x}}\pm\hat{\mathbf{y}}(\pm\hat{\mathbf{x}}\pm 2\hat{\mathbf{y}})}\rangle: \quad \tilde{E}_1+\hat{E}_1\rightarrow\tilde{E}_1+\hat{E}_1+\frac{24}{12}J. \quad \text{(A13)}$$

APPENDIX B

We list here rules that connect diagrams with matrix elements. Diagrams correspond in a self-evident way to all types of contributions described in the main body of the text. An important rule that has not been mentioned before follows from the definition of spin bag states. It states that each nontrivial contribution to an element of the overlap matrix (and to the Hermitian conjugate to it) that couples two spin bag states induces contributions to the equivalent element of the Hamiltonian matrix related to the action of the hopping term on one of coupled spin bag states, which may be chosen in an arbitrary way.

Rules for matrix elements $N_{\{i,j\},\{\varnothing\};\{i',j'\},\{\varnothing\}}$, $H_{\{i,j\},\{\varnothing\};\{i',j'\},\{\varnothing\}}$ and Figs. 3–15. (The sites i, i' belong to the even sublattice, while j, j' to the odd):

(i) Open circles represent the sites i, j; solid circles represent the sites i', j'.

(ii) The contribution to a matrix element is a product of amplitudes $\alpha_{\{(i,\mathcal{P}_i),(j,\mathcal{P}_j)\},\{\varnothing\}}$ and $\alpha_{\{(i',\mathcal{P}_{i'}),(j',\mathcal{P}_{j'})\},\{\varnothing\}}$ for ''string'' states $|\{(i,\mathcal{P}_i),(j,\mathcal{P}_j)\},\{\varnothing\}\rangle$ and $|\{(i',\mathcal{P}_{i'}),(j',\mathcal{P}_{j'})\},\{\varnothing\}\rangle$ represented by the left and middle parts of a diagram.

(iii) If the final position of a hole which started from the site i is the same as the final position of a hole which started from the site j', the contribution is multiplied by -1.

(iv) A contribution to an element of the overlap matrix is

accompanied by a contribution to an element of the Hamiltonian matrix that couples the same spin bag states. Its value is given by the contribution to the overlap matrix multiplied by the eigenenergy of that spin bag state that is the object of action of the hopping term in diagrams related to contributions to the kinetic energy.

(v) A bent arrow denotes action of the hopping term on the string state and contributes an additional factor $-t$ to the matrix element.

(vi) A pair of slanted crosses at two nearest-neighbor sites denotes action of the exchange term in the Hamiltonian and contributes a factor $J/2$ to the matrix element.

(vii) The direct contribution from each diagram should be expanded by contributions from string states that may be obtained by applying repeatedly the operators $T_{\langle i,j\rangle}$ to the common configuration of holes and spins that simultaneously corresponds to the left and middle parts of each diagram. That construction of new string states must not disturb the mechanism of the underlying process, and therefore positions of holes and spins that are objects of the Hamiltonian action must not be changed.

(viii) Contributions related to fictitious overlap and fictitious processes are additionally multiplied by -1.

(ix) Amendments related to the diagonal term in the Hamiltonian [like Fig. 9(a)] are given by a contribution from the overlap multiplied by $-J/2$ times number of broken bonds which contribution is ''saved'' due to special shape of strings.

Modifications of some rules for the matrix elements $N_{\{m,n\},\{l\};\{m',n'\},\{l'\}}$, $H_{\{m,n\},\{l\};\{m',n'\},\{l'\}}$ and Figs. 6–15 are as follows:

(i) Open circles represent the sites m, n; solid circles represent the sites m', n'. An open diamond corresponds to the site l, while a solid diamond to the site l'. (ii) The contribution to a matrix element is a product of amplitudes $\alpha_{\{(m,\mathcal{P}_m),(n,\mathcal{P}_n)\},\{l\}}$ and $\alpha_{\{(m',\mathcal{P}_{m'}),(n',\mathcal{P}_{n'})\},\{l'\}}$ for string states represented by the left and middle parts of a diagram. (iii) An initial position m is called by definition ''left-sided'' if m obeys the relation $\mathbf{R}_m-\mathbf{R}_l=\pm\hat{\mathbf{x}}$ for a spin bag state $|\{m,n\},\{l\}\rangle=|\Phi^{(1)}_{l;\pm\hat{\mathbf{x}}\pm,\hat{\mathbf{y}}}\rangle$ or if $|\{m,n\},\{l\}\rangle=|\Phi^{(2)}_{m;\pm\hat{\mathbf{x}}\pm\hat{\mathbf{y}},\pm2\hat{\mathbf{x}}\pm\hat{\mathbf{y}}(\pm\hat{\mathbf{x}}\pm2\hat{\mathbf{y}})}\rangle$. The other initial position is called by definition right-sided. If the final position of a hole that started from a left-sided site is the same as the final position of a hole that started from a right-sided site, the contribution is multiplied by -1.

Diagrams we use in the paper may be very easily transformed into standard interaction vertices. In such a case open and solid circles may be interpreted as creation and annihilation operators, respectively. Information about the configuration of involved sites should be put into the indices of fermionic operators.

[1] S.C. Zhang, Science **275**, 1089 (1997).
[2] S. Meixner, W. Hanke, E. Demler, and S.C. Zhang, Phys. Rev. Lett. **79**, 4902 (1997).
[3] R. Eder, W. Hanke, and S.C. Zhang, Phys. Rev. B **57**, 13 781 (1998).
[4] R. Eder and Y. Ohta, Phys. Rev. B **51**, 11 683 (1994).
[5] R. Eder, Y. Ohta, and S. Maekawa, Phys. Rev. Lett. **74**, 5124 (1995).
[6] J.R. Schrieffer, X.G. Wen, and S.C. Zhang, Phys. Rev. B **39**, 11 663 (1989).
[7] B.I. Shraiman and E.D. Siggia, Phys. Rev. Lett. **60**, 740 (1988).
[8] S.A. Trugman, Phys. Rev. B **37**, 1597 (1988); **41**, 892 (1990).
[9] I. Inoue and S. Maekawa, J. Phys. Soc. Jpn. **59**, 2110 (1990).
[10] E. Dagotto and J.R. Schrieffer, Phys. Rev. B **43**, 8705 (1990).
[11] S. Nishimoto, Y. Ohta, and R. Eder, Phys. Rev. B **57**, R5590 (1998).
[12] E. Dagotto, A. Nazarenko, and A. Moreo, Phys. Rev. Lett. **74**, 310 (1995).
[13] R. Eder, Phys. Rev. B **45**, 319 (1992).
[14] M.Yu. Kuchiev and O.P. Sushkov, Physica C **218**, 197 (1993).
[15] R. Eder and K.W. Becker, Z. Phys. B **78**, 219 (1990).
[16] P. Wróbel and R. Eder, Phys. Rev. B **49**, 1233 (1994).
[17] P. Wróbel and R. Eder, Phys. Rev. B **54**, 15 882 (1996).
[18] B. Batlogg *et al.*, Physica C **235**, 130 (1994).
[19] L.N. Bulaevskii, E.L. Nagaev, and D.L. Khomskii, Zh. Éksp. Teor. Fiz. **54**, 1562 (1968) [Sov. Phys. JETP **27F**, 836 (1968)].
[20] Y. Hasegawa and D. Poilblanc, Phys. Rev. B **40**, 9035 (1989).
[21] D. Poilblanc, Phys. Rev. B **49**, 1477 (1994).
[22] M. Bonnisegni and E. Manousakis, Phys. Rev. B **47**, 11 897 (1993).
[23] W.O. Putikka, M.U. Luchini, and T.M. Rice, Phys. Rev. Lett. **68**, 538 (1992); W.O. Putikka, M.U. Luchini, and M. Ogata, *ibid.* **69**, 2288 (1992).
[24] E. Dagotto, Rev. Mod. Phys. **66**, 763 (1994).
[25] V.I. Belinicher, A.L. Chernyshev, A.V. Dotsenko, and O.P. Sushkov, Phys. Rev. B **51**, 6076 (1995); V.I. Belinicher, A.L. Chernyshev, and V.A. Shubin, *ibid.* **56**, 3381 (1997).
[26] S.R. White and D.J. Scalapino, Phys. Rev. B **55**, 6504 (1997).
[27] J. Riera and E. Dagotto, Phys. Rev. B **57**, 8609 (1998).
[28] J.M. Tranquada, B.J. Sternlieb, J.P. Axe, Y. Nakamura, and S. Uchida, Nature (London) **375**, 561 (1995).